

Dissertation

Vortex structure in anisotropic and
quantum-limit superconductors

Nobuhiko Hayashi ¹

1999

The Graduate School of
Natural Science and Technology
Okayama University
Japan

¹E-mail : hayashi@mp.okayama-u.ac.jp
URL : <http://mp.okayama-u.ac.jp/%7Ehayashi/vortex.html>

Dedicated to Dr. Harald F. Hess

Abstract

Electronic structure of a single vortex (or vortex core structure) in type-II superconductors is theoretically discussed in the present thesis. Low-lying excited states in the superconductors due to the vortex, i.e., “vortex bound states,” are examined in detail on the basis of numerical calculations. Two points are focused on: the effect of *superconducting gap anisotropy* on a vortex (Chapter 2) and the property of a vortex in *quantum-limit* situation (Chapter 3).

The anisotropy of a superconducting energy gap has substantial effects on the structure of the vortex bound states. The local density of states around a vortex is calculated in a clean superconductor with the gap anisotropy within the framework of the quasiclassical theory of superconductivity. A characteristic structure of the local density of states, observed experimentally in the layered hexagonal superconductor $2H\text{-NbSe}_2$ by scanning tunneling microscopy (STM), is well reproduced by assuming an *anisotropic s-wave* gap. The local density of states (or the bound states) around a vortex in superconductors with gap anisotropy is interpreted in terms of quasiparticle trajectories to facilitate an understanding of the rich electronic structure observed in STM experiments. This reveals not only a rich internal electronic structure associated with a vortex core, but also unique ability of the STM spectroscopy.

The quantum limit means that the superconducting coherence length is small in the limit, i.e., it is comparable to the atomic length order. Focusing on quantum-limit behavior, fundamental structure of a vortex is studied by self-consistently solving the Bogoliubov-de Gennes equation. The discreteness of the energy levels of the vortex bound states is crucial for the vortex structure in the quantum limit. The following are revealed by the study of the quantum limit. The vortex core radius shrinks monotonically up to an atomic-scale length on lowering the temperature T , and the shrinkage stops to saturate at a lower T . The pair potential, supercurrent, and local density of states around the vortex exhibit Friedel-like oscillations. The local density of states inside a vortex core generally has particle-hole asymmetry induced by the existence of the vortex itself.

Some essential properties of general vortices which are concealed within the conventional non-quantum-limit analysis can be extracted by the quantum-limit analysis. On the basis of the inherent particle-hole asymmetry inside vortex cores, it is discussed in this thesis that electric charging of a vortex core is originated from the Friedel oscillation of the Bogoliubov wave functions around the vortex (Chapter 4). This mechanism of the vortex core charging is independent of the slope in the normal-state density of states at the Fermi level. The temperature dependence of the vortex core charge is also presented. It is expected that by using STM, information on the vortex core charging is extracted through a

relation between the vortex core charge and the vortex bound states.

List of Papers

Main work

- “Star-shaped local density of states around vortices in a type-II superconductor,”
N. Hayashi, M. Ichioka, and K. Machida, Phys. Rev. Lett. **77**, 4074 (1996).
- “Effects of gap anisotropy upon the electronic structure around a superconducting vortex,”
N. Hayashi, M. Ichioka, and K. Machida, Phys. Rev. B **56**, 9052 (1997).
- “Low-lying quasiparticle excitations around a vortex core in quantum limit,”
N. Hayashi, T. Isoshima, M. Ichioka, and K. Machida, Phys. Rev. Lett. **80**, 2921 (1998).
- “Relation between vortex core charge and vortex bound states,”
N. Hayashi, M. Ichioka, and K. Machida, J. Phys. Soc. Jpn. **67**, 3368 (1998).

Others

- “Fundamental properties of a vortex in a d -wave superconductor,”
M. Ichioka, N. Hayashi, N. Enomoto, and K. Machida, J. Phys. Soc. Jpn. **64**, 4547 (1995).
- “ s - and d_{xy} -wave components induced around a vortex in $d_{x^2-y^2}$ -wave superconductors,”
M. Ichioka, N. Enomoto, N. Hayashi, and K. Machida, Phys. Rev. B **53**, 2233 (1996).
- “Vortex core structure and possible pairing mixture in d -wave superconductors,”
K. Machida, M. Ichioka, N. Hayashi, and N. Enomoto, Physica C **263**, 428 (1996).
- “Vortex structure in d -wave superconductors,”
M. Ichioka, N. Hayashi, N. Enomoto, and K. Machida, Phys. Rev. B **53**, 15316 (1996).
- “Local density of states in the vortex lattice in a type-II superconductor,”
M. Ichioka, N. Hayashi, and K. Machida, Phys. Rev. B. **55**, 6565 (1997).

- “Vortex structure in anisotropic superconductors,”
M. Ichioka, N. Hayashi, and K. Machida, *BUTSURI (Physics)* **53**, No. 8, 611 (1998) [in Japanese].
- “Vortex structure in clean type-II superconductors with s-wave and d-wave pair symmetries,”
K. Machida, M. Ichioka, N. Hayashi, and T. Isoshima, in *The Superconducting State in Magnetic Fields: Special Topics and New Trends*, edited by C. A. R. Sá de Melo (World Scientific, Singapore, 1998), Chap. 13, p. 245.

Contents

1	Introduction to Vortex	9
1.1	Type-II Superconductor and Vortex	9
1.2	Vortex Bound States	10
1.3	Open questions of the vortex structure observed by STM experiments	11
2	Effects of Gap Anisotropy on the Vortex Structure	19
2.1	Introduction	19
2.2	The quasiclassical theory of superconductivity	21
2.3	Pair potential and local density of states	24
2.3.1	Pair potential	25
2.3.2	Local density of states	25
2.4	Quasiparticle trajectories	34
2.4.1	Direction-dependent local density of states	34
2.4.2	Interpretation on the LDOS around a vortex	35
2.4.3	Flows of quasiparticles around a vortex	38
2.5	Summary and discussions	38
2.5.1	Comparison with other theories and effects of the vortex lattice	40
2.5.2	Beyond the quasiclassical approach	41
2.5.3	Concluding remarks	42
3	Quantum-Limit Property of a Vortex	43
3.1	Introduction	43
3.2	Bogoliubov-de Gennes theory	44
3.3	Results	45
3.4	Summary	50
4	Electric Charging of a Vortex Core	51
4.1	Introduction	51
4.2	Formulation	53
4.3	Results	54
4.4	Discussions	57
4.5	Summary	57
5	Conclusion	59

Chapter 1

Introduction to Vortex

In the present chapter, I shall give a brief introduction to vortices in type-II superconductors and mention “vortex bound states” discussed in the following chapters. Open questions of the related experimental results will be pointed out.

1.1 Type-II Superconductor and Vortex

Superconductors under magnetic fields exhibit the so-called Meissner-Ochsenfeld effect, that is, the magnetic fields applied to superconducting material are expelled from the inside of the material. Some superconductors, called “type I,” exhibit a perfect Meissner-Ochsenfeld effect up to a critical field H_c , and at this critical field the transition to the normal state suddenly takes place. In the other superconductors, called “type II,” magnetic fields are expelled up to a lower critical field H_{c1} , and at an upper critical field H_{c2} the superconductivity is broken. In the intermediate field region $H_{c1} < H < H_{c2}$, the magnetic field partly penetrates into the material *keeping the superconductivity*. The magnetic fields penetrate into the superconductors in the form of quantized flux lines. The quantized flux lines exhibit characteristic phenomena in type-II superconductors, and a system constituted of such flux lines has a variety of physical aspects.

Around the flux line, the supercurrent circularly flows and a quantity which characterizes the superconductivity, i.e., the order parameter of superconductivity (a complex quantity), varies by $2\pi n$ in its phase. (n is an integer.) The structure of such a flux line is called “vortex,” and the superconducting state at $H_{c1} < H < H_{c2}$ is called “vortex state” (and frequently called “mixed state” traditionally). In the present thesis, I will reveal the rich structure of individual vortex (or the structure of vortex core) in type-II superconductors. The essence of this study would provide implications for vortices in fermionic superfluid systems such as the superfluid ^3He . Studies of vortices in superconductors under magnetic fields could also be important from the applied physics point of view in general. (For a historical review of the type-II superconductors, refer to Ref. [1] and Sec. 1 of Ref. [2] for example.)

1.2 Vortex Bound States

The superconducting state is an ordered state with symmetry breaking. The superconductivity is characterized by a quantity (i.e., the order parameter), $\langle aa \rangle$, symbolically. Here a is the annihilation operator for the fermionic quasiparticles and $\langle \rangle$ means the thermal average. In the superconducting state $\langle aa \rangle \neq 0$, and, on the other hand, $\langle aa \rangle = 0$ in the normal state. Thus the U(1) gauge symmetry is broken in the superconducting state ($\langle aa \rangle \neq 0$). ($\langle aa \rangle$ is not U(1) gauge invariable. That is, $\langle aa \rangle \rightarrow \langle aa \rangle \exp[2i\theta] (\neq \langle aa \rangle)$, when $a \rightarrow a \exp[i\theta]$ and $a^\dagger \rightarrow a^\dagger \exp[-i\theta]$.) Now, it is a crucial point that the modulus of that quantity, $|\langle aa \rangle|$, determines an energy gap in the excitation spectrum of the superconducting state. Let us define the superconducting order parameter as Δ whose modulus $|\Delta|$ gives the magnitude of the energy gap due to superconductivity.

When Δ has a spatial dependence in superconductors, what does take place there? The vortex state is one of the typical situations where Δ varies spatially in superconducting material. In analogy, let us consider a hetero junction in semiconductors. It is well known that when semiconductors with different energy gaps are joined each other, a quantum well is constituted there. Similarly, in superconductors, it is expected that if the superconducting gap $|\Delta|$ has a spatial dependence, a kind of the quantum well should be constituted and the quantized energy levels due to the well should appear there. Around a vortex, the phase of the order parameter Δ varies by 2π with a rotation about the vortex center; it means that one quantum flux penetrates there. When we take the z axis in the direction of the flux line in cylindrical coordinates $\mathbf{r} = (r, \theta, z)$, the order parameter Δ around a vortex is expressed as $\Delta(\mathbf{r}) = \Delta(r) \exp[i\theta]$. Because of the indeterminacy of the phase factor $\exp[i\theta]$ at the vortex center $r = 0$, the magnitude part becomes $\Delta(r = 0) = 0$ inevitably. Thus the gap $\Delta(r)$ is $\Delta(0) = 0$ at the vortex center, and far from the vortex it recovers to the uniform value Δ_∞ . This spatial structure of the energy gap gives rise to low-energy bound states below the gap around a vortex as in the quantum well systems.

The existence of the low-energy bound states around a vortex was first discussed theoretically in 1964 by Caroli, de Gennes, and Matricon[3]. Energy spectra in spatially inhomogeneous superconductors can be obtained as the eigenenergy spectra of the Bogoliubov-de Gennes (BdG) equation[4]. The BdG equation corresponds to the Schrödinger equation for superconducting systems. Caroli *et al.*[3] applied the BdG equation to a vortex system. They solved the equation analytically by simplifying the problem. As a result, they found low-energy excited states bounded around the vortex. These bound states due to vortices are called “vortex bound states,” or “Caroli-de Gennes-Matricon states,” or rarely “chiral branch.” The vortex bound states can have important effects on the thermodynamics and transport in superconductors under magnetic fields.

Theoretically, after the seminal work by Caroli *et al.*[3], several theorists studied the electronic structure around vortices and its effects on physical phenomena. Experimentally, nevertheless, there had existed for a long time no experiments which could directly study the electronic structure around vortices[5]. In 1989, however, Hess *et al.*[6] first succeeded in experimentally observing the electronic structure around vortices. They investigated the energy spectra around vortices by a point-contact tunneling current probe with an atomic-scale

spatial resolution, i.e., the scanning tunneling microscope (STM). The tunneling current I of the “normal state/insulator/(s -wave) superconductor (NIS)” junction is given as[7]

$$I(V) \propto \int_{-\infty}^{\infty} dE N(E) \{f(E) - f(E + eV)\}, \quad (1.1)$$

where $N(E)$ is the density of states in the superconductor, V is the bias voltage applied to the junction, and $f(E)$ is the Fermi function. Differentiating Eq. (1.1) about V , one obtains the differential conductance,

$$\frac{dI(V)}{dV} \propto \int_{-\infty}^{\infty} dE N(E) \left\{ -\frac{df(E + eV)}{dV} \right\}. \quad (1.2)$$

The derivative of the Fermi function becomes very sharply peaked at $E = -eV$ at low temperatures as if it is the delta function. Equation (1.2) means that we can obtain the density of states $N(E)$ of the superconductor by measuring the differential conductance dI/dV at sufficiently low temperatures. The spatial resolved probe, STM, enables us to measure dI/dV at each position on the surface of the superconductor, so that we can obtain the local density of states $N(\mathbf{r}, E)$ of the superconductor[8].

In absence of vortices, or sufficiently far from a vortex, the BCS energy gap should appear in the energy spectra. Near the vortex center, on the other hand, finite density of states was expected to exist inside the gap, due to the above mentioned low-energy bound states (i.e., the vortex bound states) around a vortex. In Figs. 1.1 and 1.2, shown is the experimental results for the energy spectra at the vortex center and at some distance from it, observed first with STM in 1989 by Hess *et al.*[6] The superconducting material used in the experiment was a clean type-II superconductor, the layered hexagonal compound $2H\text{-NbSe}_2$ [8]. The BCS gap is certainly recovered far from the vortex center. It was, those days, surprising that an unexpected large peak appeared in the experimentally observed data at the zero bias voltage at the vortex center. According to the experimental result, the above mentioned vortex bound states not only filled the gap on the vortex, but also gave the characteristic peak structure at the vortex center. It was later called the “zero-bias peak” at the vortex center. Actually this peak originates just from the vortex bound state which belongs to the lowest eigenenergy $E_{1/2}$ of Caroli *et al.* (Strictly speaking[9], this large peak is composed of the $u_{1/2}$ component of the Bogoliubov wave function (u, v) [4] which belongs to $E_{1/2}$. The component $v_{1/2}$, on the other hand, never constitutes the large peak at $E_{1/2}$, but just contributes to a smaller peak at $E = -E_{1/2}$. This point is crucial for revealing concealed properties of vortices such as the electric charging of the vortex core[10]. I will discuss them in the chapter 3 and 4.) In the next section, I point out the open questions of vortices related to the STM experiments which I will deal with in the present thesis.

1.3 Open questions of the vortex structure observed by STM experiments

As mentioned in the preceding section, Hess *et al.*[6] succeeded in observing the electronic structure around vortices in NbSe_2 . They further advanced the investigation and revealed that a vortex had rich and complicated properties in its

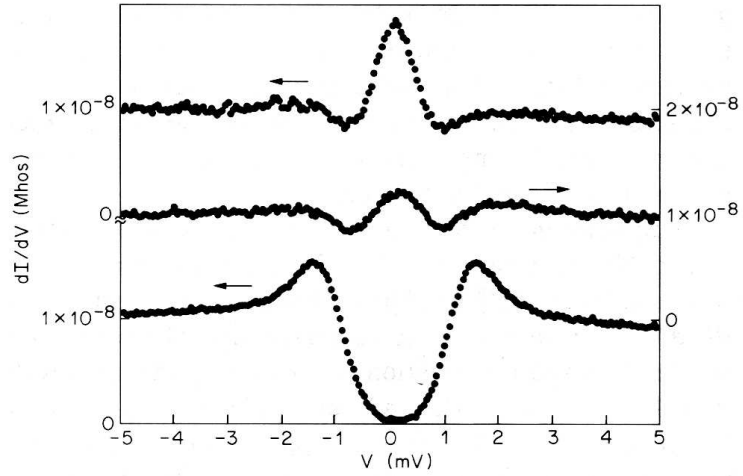


Figure 1.1: dI/dV vs V for NbSe_2 at 1.85 K and a 0.02-T field, taken at three positions: on a vortex (top curve), about 75 Å from a vortex (middle), and 2000 Å from a vortex (bottom). The zero of each successive curve is shifted up by one quarter of the vertical scale. (From Ref. [6].)

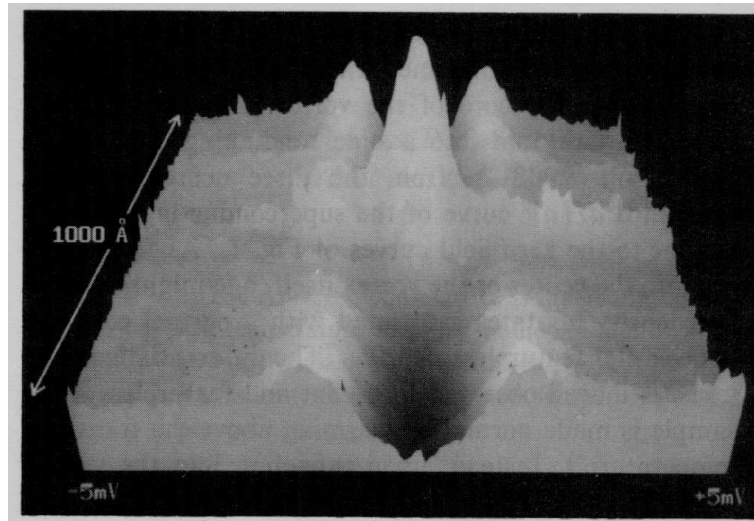


Figure 1.2: Perspective image of dI/dV vs tunneling voltage (horizontal axis) and position along a line that intersects a vortex (vertical axis). Cross sections of this image at a few positions are shown in Fig. 1.1. (From Ref. [6].)

electronic structure. After the first experimental success by Hess *et al.*, several theoretical studies of the electronic structure around a vortex were prompted by the STM experiment. Shore *et al.*[11] numerically solved the BdG equation first to obtain all the vortex bound states below the gap in order to explain the zero-bias peak observed in the STM experiment. As a result, they not only explained the existence of the zero-bias peak at the vortex center, but also found an energy shift of the peak at a distance from the vortex center[11]. Their numerical result showed that the zero-bias peak appeared at the vortex center and the peak split into two (positive and negative energy peaks) at some distance from the vortex center. This feature can be understood as follows. If quasiparticles rotate on the vortex line, the quasiparticles have the angular momentum μ about the vortex center. When μ is expressed as $\mu = p_F r$, the quasiparticles with larger μ circulate farther away from the vortex center (p_F is the Fermi momentum and r is the radial distance of the quasiparticle from the vortex center). The quasiparticle with the larger angular momentum may have the larger energy. It is then expected that the energy of the quasiparticle is proportional to the radial distance from the vortex center, i.e., the quasiparticles circulate farther away from the vortex center as they have higher energy. The result obtained by Shore *et al.*[11] reflected just this dispersion relation of the quasiparticle around a vortex. (Note that the electron-like (hole-like) quasiparticle around a vortex corresponds to the positive (negative) energy peak.) After this theoretical prediction[11] was made, Hess *et al.*[12] attempted to observe such a splitting of the peak around a vortex and eventually confirmed the prediction successfully [Fig. 1.3]. Up to this point, so nice coincidence between experiment and theory had been achieved.

However, a stimulating mystery also emerged at that time. In the above experiment, Hess *et al.*[12] not only confirmed the splitting, but also found that the STM imaging of a vortex (or the local density of states around a vortex) was shaped like a “star” at a fixed energy and its orientation was dependent on the energy, i.e., the sixfold star shape rotates as the bias voltage varies [Fig. 1.4] (Fig. 4 in Ref. [12]). In the intermediate energy, a “ray” of the star splits into a pair of nearly parallel rays [0.24 mV data in Fig. 1.4] (Fig. 1 in Ref. [13] or Fig. 1 in Ref. [14]). A more detailed and lower-temperature investigation also revealed later that the zero-bias peak in the spectral evolution along a radial line from the vortex center does not split into two subpeaks observed in the earlier experiment, but into three or more ones [Figs. 1.5, 1.6, and 1.7] (Figs. 9 and 10 in Ref. [8], or Fig. 6 in Ref. [15]).

These beautiful experimental observations by Hess *et al.* revealed that vortices had rich electronic structure, which may be related to the thermodynamic and transport properties of superconductors under magnetic fields. Their STM experiments shed a new light on the physics of vortices. Yet, there have been no sufficient theories which could explain these experimental results, although a seminal developing idea has been proposed at the early stage. Such a theoretical situation for the experimental results of the electronic structure around vortices may have impeded the progress of this field. It has been desired that further theoretical development from the early work should be advanced to break the deadlock.

The most thorough theoretical study of a vortex was given in a paper by Gygi and Schlüter[16] in 1991. Fundamental properties of a vortex were discussed in their paper on the basis of beautiful results of ingenious numerical

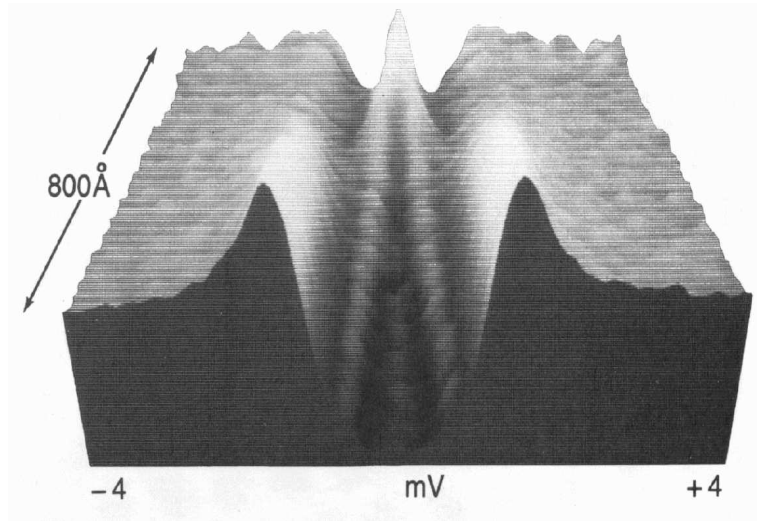


Figure 1.3: Perspective view of the superconducting spectra as it evolves on an 800 Å line that penetrates through a vortex. Notice the zero-bias peak at the vortex center and how it splits into two subgap peaks at larger radius from the core. (From Ref. [8].) Note also that *the evolution of the split peaks along radial line represents a dispersion relation between the energy E (or bias voltage) and the angular momentum μ (or radial distance r) of the quasiparticles around the vortex center.*

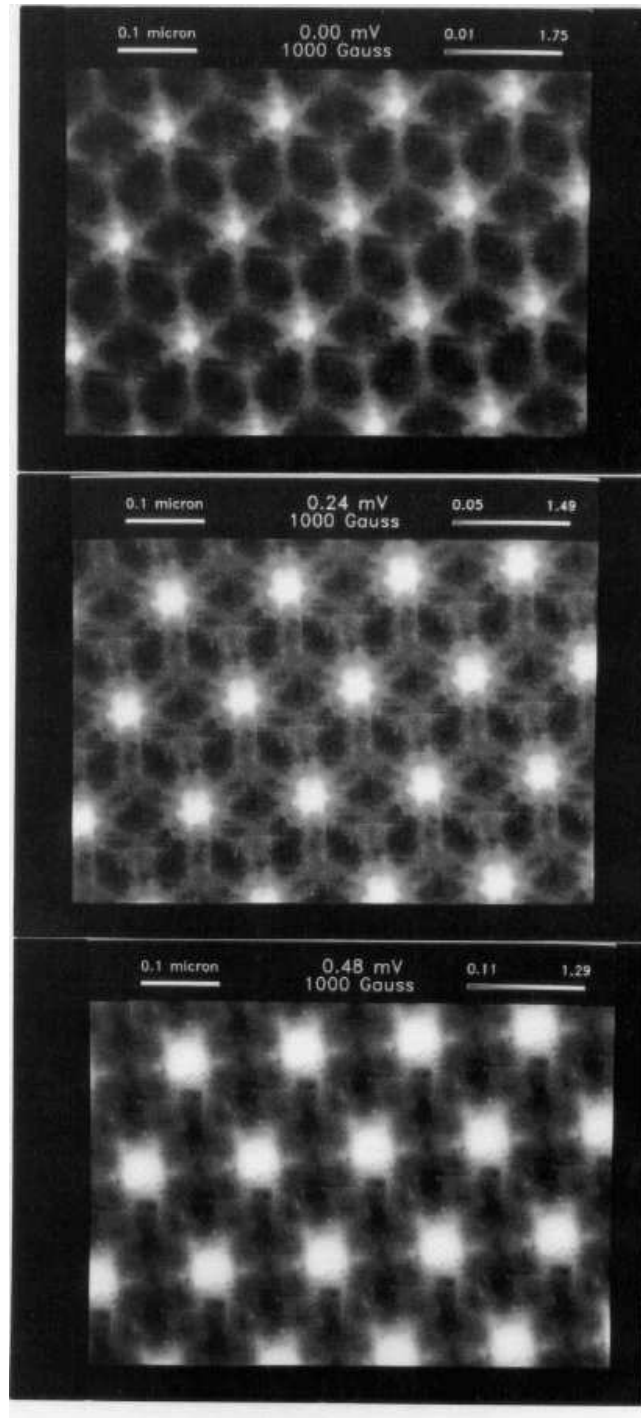


Figure 1.4: Real space images of vortices in NbSe₂ generated by measuring the differential conductance $dI/dV(x, y, V)$ at each fixed bias voltage V (from Ref. [13]).

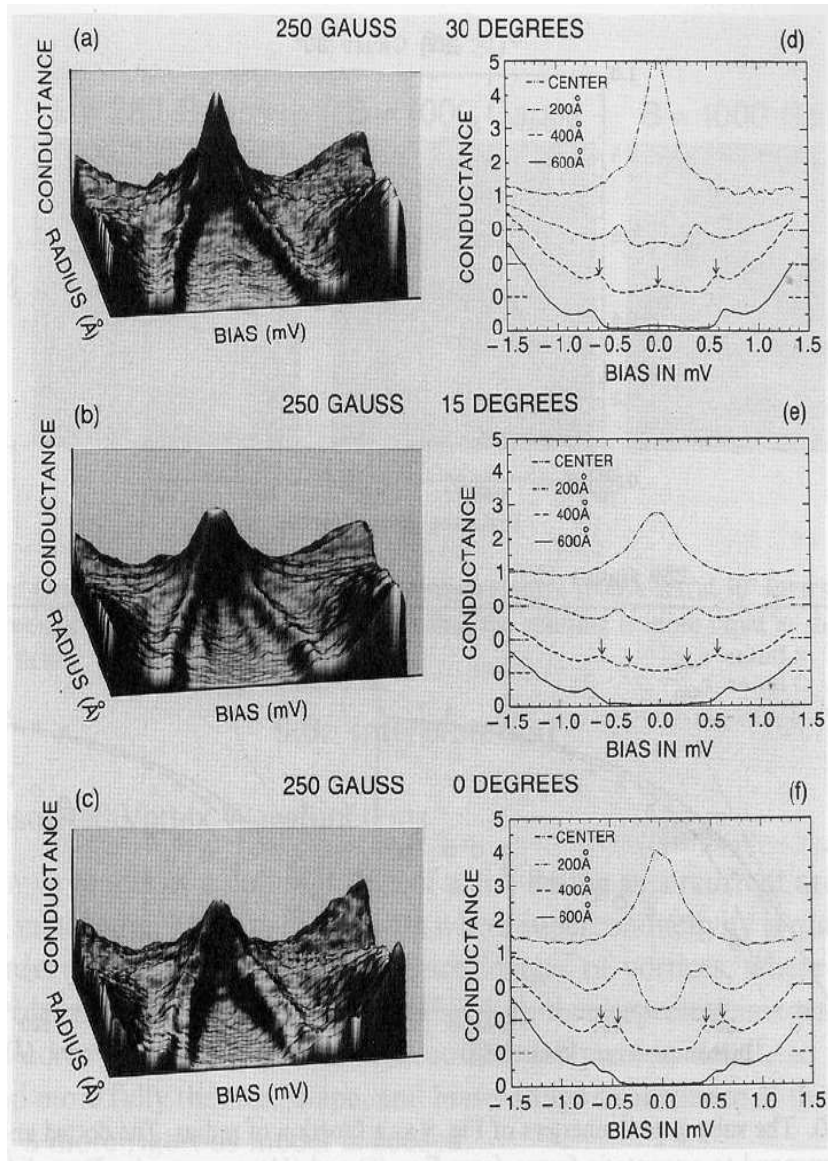


Figure 1.5: A detailed perspective of $dI/dV(V, r)$ (at 50 mK) showing how it evolves along the three lines sketched in Fig. 1.6. The perspective scale corresponds to a 1000 Å sampling line with the vortex positioned at 250 Å from the back. The outer subgap peak is not sensitive to angle, but the inner peak collapses to zero energy at 30°. A few spectra of the perspective data are explicitly plotted in Figs. 1.5(d), 1.5(e), and 1.5(f). (From Ref. [8].)

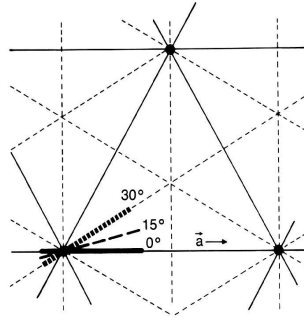


Figure 1.6: Schematic of the various sampling lines that pass through the vortex core and are used for the spectral evolution data of Figs. 1.5 and 1.7. The crystallographic a direction is indicated and lines up also with the vortex lattice direction. (From Ref. [8].)

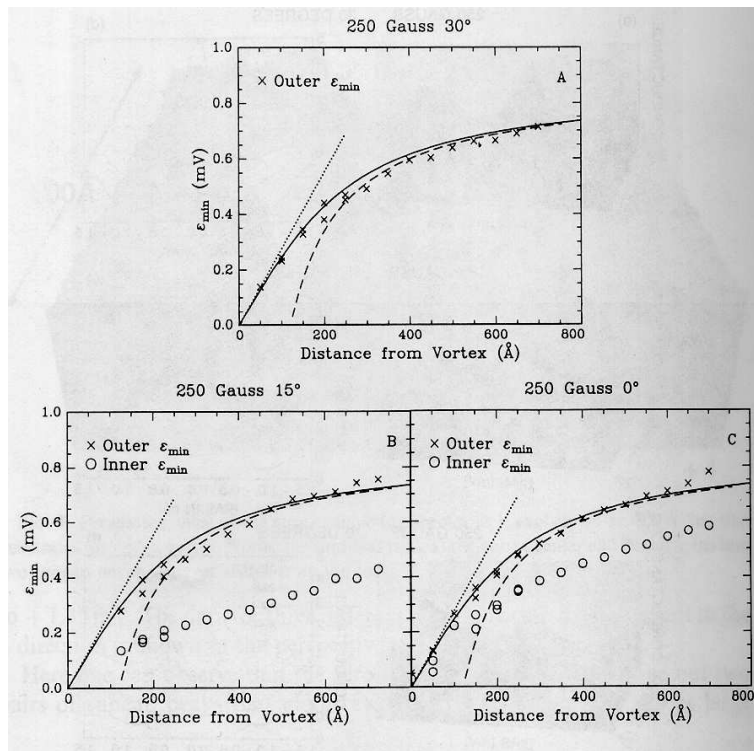


Figure 1.7: The subgap peak energies of Fig. 1.5 as a function of radius. The solid line is a guide corresponding to the outer subgap peak data. (From Ref. [8].)

calculations. Every time I read that paper, I can find significant results renewedly and learn much from it. That study is truly excellent work and most essence of a vortex is contained in their paper, from which we can get inspiration to investigate various physics of vortices. Simultaneously, however, an issue under developing those days was also discussed there. I should point out that this issue was just the above mentioned anisotropic electronic structure around the vortex observed by the STM experiments. While part of the features of the experimental results could be captured by a developing analysis by them[17], further theoretical development is hopefully expected to be advanced. In fact, a consistent understanding of both the star-shaped structure and the anisotropic spectral evolutions along radial lines mentioned above has been lacking during these past years. I have tackled this problem, and found that the rich electronic structure observed in the STM experiments (Refs. [12, 13, 14, 8, 15]) was able to be understood in a natural way in terms of superconducting gap anisotropy in the k space. From a more general point of view, it is found that the complicated electronic structure around the vortex can be consistently understood with “quasiparticle trajectories” from the viewpoint of the quasiclassical theory of superconductivity. I will discuss them in the chapter 2.

Another current open question of vortices is the electronic structure around vortices in high- T_c cuprate superconductors. The high- T_c cuprates have given us many challenging problems in various fields of physics. Peculiar electronic structure inside the vortex in these compounds observed recently by a few STM experiments[18, 19] is one of the puzzling (but, interesting) properties of the high- T_c superconductors. This problem is currently debated on with some confusing. The point may be twofold for the present: (a) a probable anisotropic (or unconventional) pairing of the Cooper pair (e.g., d -wave superconductivity), and (b) a *quantum-limit* property, i.e., a possible existence of the short coherence length ξ of superconductivity comparable to the atomic length order $1/k_F$ (k_F is the Fermi wave number). As a first step to elucidate the vortex structure in the high- T_c cuprates, I investigate the fundamental properties of a vortex in the quantum limit ($k_F\xi \sim 1$). I will discuss it in the chapter 3. Focusing on the quantum limit, I can reveal the concealed properties of vortices, e.g., the electric charging of vortices. In the chapter 4, I will discuss the vortex core charge as an inherent property of general vortices.

The detailed background and motivation of my work in the present thesis will also be given in the introductory sections of each following chapter.

Chapter 2

Effects of Gap Anisotropy on the Vortex Structure

2.1 Introduction

The existence of an anisotropy of a superconducting energy gap has attracted a great deal of attention in various superconductors such as heavy fermion, organic, and high- T_c compounds. On the other hand, the electronic structure around vortices is a fundamental problem on the physics of both conventional and unconventional superconductors. In this chapter, we discuss effects of the gap anisotropy upon the electronic structure around a vortex, i.e., the bound states around an isolated vortex in clean type-II superconductors.

Theoretically, the bound states around a vortex was discussed in 1964 by Caroli, de Gennes, and Matricon[3], who considered a single vortex in an isotropic s -wave superconductor. After this work, several theorists studied the electronic structure around vortices (e.g., Refs. [20, 21, 22, 23, 24]). Experimentally, however, until the following success by Hess *et al.*, there had existed for a long time no experiments which could directly study the electronic structure around vortices[5].

In 1989, a novel experimental method, scanning tunneling microscopy (STM), opened up a way to study the electronic structure around vortices in type-II superconductors[5, 8]. Using the STM method, Hess *et al.*[6] succeeded in measuring spatially resolved excitation spectra, i.e., local density of states (LDOS) around a vortex. They investigated the bound states around a vortex in the layered hexagonal compound $2H$ -NbSe₂ ($T_c=7.2$ K), and found a striking zero-bias peak at the vortex center. Later the same peak and its collapse upon substituting Ta for Nb as impurities in NbSe₂ were also observed by Renner *et al.*[25, 26] Several new theoretical studies of the electronic structure around a vortex [27, 28, 11, 29, 16, 30, 31, 32, 33] were prompted by the success of the STM experiment by Hess *et al.*[6] Some of these theories[11, 16, 30, 31, 32] predicted that the zero-bias peak should split into two, i.e., into positive and negative bias voltage peaks, if spectra are taken at some distance from the vortex center (see, for instance, Fig. 3 in Ref. [11]). This splitting indicates that quasiparticles of the vortex bound states with finite angular momentum are distributed circularly, and circulate farther away from the core center as

they have higher energy. The predicted splitting was actually confirmed in an experiment.[12]

However, a mystery also emerged. In the above experiment, Hess *et al.*[12] not only confirmed the splitting, but also found that the LDOS around the vortex was shaped like a “star” at a fixed energy and its orientation was dependent on the energy, i.e., the sixfold star shape rotates as the bias voltage varies [Fig. 1.4] (Fig. 4 in Ref. [12]). Soon after this observation was made, Gygi and Schlüter[17] proposed an explanation for this 30° rotation of the star-shaped LDOS. On the basis of a sixfold perturbation, they explained that the two states, i.e., the lower and higher energy stars were interpreted as bonding or antibonding states[17]. Although they explained certain aspects of the observation, the following features of the star-shaped LDOS observed in later experiments[13, 14, 8, 15] could not be sufficiently understood by this perturbation scheme. In the intermediate energy, a “ray” of the star splits into a pair of nearly parallel rays [0.24 mV data in Fig. 1.4] (Fig. 1 in Ref. [13] or Fig. 1 in Ref. [14]). The zero-bias peak in the spectral evolution along a radial line from the vortex center does not split into two subpeaks observed in the earlier experiment, but into three or more ones [Figs. 1.5, 1.6, and 1.7] (Figs. 9 and 10 in Ref. [8], or Fig. 6 in Ref. [15].)

Specifically, the characteristic features of the LDOS observed in NbSe₂ (Refs. [12, 13, 14, 8, 15]) are summarized in detail as follows, when the magnetic field H is applied perpendicular to the hexagonal plane: (1) The LDOS for quasiparticle excitations has a sixfold star shape centered at the vortex core[12]. (2) The orientation of this star depends on the energy. At zero bias, a ray of the star extends away from the a axis in the hexagonal plane of NbSe₂. Upon increasing the bias voltage, the star rotates by 30° [Fig. 1.4]. (3) In the intermediate bias voltage, a ray splits into a pair of nearly parallel rays, keeping its direction fixed [0.24 mV data in Fig. 1.4] [13, 14]. (4) In the spectral evolution which crosses the vortex center, there exist inner peaks in addition to the outer peaks which evolve from the zero bias peak at the vortex center into the bulk BCS like gap edges far from the vortex [Figs. 1.5, 1.6, and 1.7] [8, 15]. The inner peaks vary with the angle of the direction in which the spectral evolution is taken. These important and interesting observations (1)–(4) remain unexplained.

Quite recently, motivated by a possibility of a d -wave superconductivity in high- T_c cuprates, Schopohl and Maki[34, 35] studied the electronic structure around a vortex in a d -wave superconductor. On the basis of the quasiclassical Green’s function theory[36, 37, 38], the LDOS around a single vortex was calculated in a superconductor with a d -wave energy gap. They found that the LDOS exhibits a characteristic fourfold structure in the d -wave gap case, which is contrasted with the isotropic s -wave gap case (a circularly symmetric LDOS)[34, 35]. A gradual 45° rotation of this fourfold LDOS as the energy changes was later reported by the present authors[39]. We note that this rotation is similar to that observed in NbSe₂[40].

In the context described above, we have investigated the electronic structure around the vortex observed in NbSe₂. We find that the rich structure of the LDOS observed in the STM experiments (Refs. [12, 13, 14, 8, 15]) results mainly from a superconducting gap anisotropy. Assuming an *anisotropic s*-wave gap analogous to the d -wave one, we are able to obtain results favorably comparable with the experiments. In a paper[41], we enumerated the following items as the possible origin of the rich structure of the LDOS: (a) the effect of an anisotropic

superconducting energy gap, (b) the effect of nearest-neighbor vortices, i.e., the effect of the vortex lattice, and (c) the effect of the anisotropic density of states at the Fermi surface. It is the purpose of the present chapter to discuss the gap effect (a) in detail. As for the item (b), i.e., the vortex lattice effect, we gave a detailed report in Ref. [42].

To date, NbSe₂ has been the only compound in which the electronic structure around vortices was thoroughly investigated by STM. In this chapter, we concentrate our attention on the LDOS observed in NbSe₂ as a typical example of a type-II superconductor. However, the essence of the present considerations is equally applicable to other type-II superconductors in general. The LDOS around a vortex reflects the internal electronic structure of the vortex, and an understanding of this structure is important in elucidating dynamical properties of vortices as well as static ones.

We consider the case of an isolated static vortex under a magnetic field applied parallel to the c axis (or z axis). We restrict ourselves to a two dimensional system, i.e., assume a two dimensional Fermi surface neglecting a small warping of the Fermi surface along the c axis, which is appropriate to layered superconductors such as NbSe₂[87, 109].

In Sec. 2.2, we describe the quasiclassical theory we use for the study of the vortex. Section 2.3 is devoted to the calculations of the LDOS around a vortex under the influence of the gap anisotropy. In Sec. 2.4, we interpret the resultant LDOS in terms of quasiparticle trajectories. The summary and discussions are given in Sec. 2.5.

2.2 The quasiclassical theory of superconductivity

To investigate the LDOS around a vortex, we use the quasiclassical Green's function theory[36, 37, 38]. The quasiclassical theory is a very powerful method, especially for spatially inhomogeneous systems such as surfaces[45, 46] and vortices[47, 48]. Furthermore, one can easily treat a superconducting gap anisotropy as well as the Fermi surface anisotropy in the quasiclassical theory. We consider the transportlike Eilenberger equation for the quasiclassical Green's function

$$\hat{g}(i\omega_n, \mathbf{r}, \bar{\mathbf{k}}) = -i\pi \begin{pmatrix} g(i\omega_n, \mathbf{r}, \bar{\mathbf{k}}) & if(i\omega_n, \mathbf{r}, \bar{\mathbf{k}}) \\ -if^\dagger(i\omega_n, \mathbf{r}, \bar{\mathbf{k}}) & -g(i\omega_n, \mathbf{r}, \bar{\mathbf{k}}) \end{pmatrix} \quad (2.1)$$

in a 2×2 matrix form (for even-parity superconductivity), namely,

$$i\mathbf{v}_F(\bar{\mathbf{k}}) \cdot \nabla \hat{g}(i\omega_n, \mathbf{r}, \bar{\mathbf{k}}) + \left[\begin{pmatrix} i\omega_n & -\Delta(\mathbf{r}, \bar{\mathbf{k}}) \\ \Delta^*(\mathbf{r}, \bar{\mathbf{k}}) & -i\omega_n \end{pmatrix}, \hat{g}(i\omega_n, \mathbf{r}, \bar{\mathbf{k}}) \right] = 0. \quad (2.2)$$

The Eilenberger equation (2.2) is supplemented by the normalization condition

$$\hat{g}(i\omega_n, \mathbf{r}, \bar{\mathbf{k}})^2 = -\pi^2 \hat{1}. \quad (2.3)$$

Here $\omega_n = (2n + 1)\pi T$ is the Matsubara frequency. The vector $\mathbf{r} = (x, y)$ is the center of mass coordinate, and the unit vector $\bar{\mathbf{k}}$ represents the relative coordinate of the Cooper pair. The overbar denotes unit vectors. The commutator $[\hat{A}, \hat{B}] = \hat{A}\hat{B} - \hat{B}\hat{A}$. We assume the Fermi velocity $\mathbf{v}_F(\bar{\mathbf{k}})$ is a function of $\bar{\mathbf{k}}$ with

reflecting the anisotropy of the Fermi surface. Since we consider an isolated single vortex in an extreme type-II superconductor where the Ginzburg-Landau parameter $\kappa \gg 1$, the vector potential can be neglected in Eq. (2.2).

The Eilenberger equation in the matrix form (2.2) can be written down to the following equations,

$$\begin{aligned} \left(\omega_n + \frac{v_F(\theta)}{2} \frac{d}{dr_{\parallel}}\right) f(i\omega_n, \mathbf{r}, \theta) &= \Delta(\mathbf{r}, \theta) g(i\omega_n, \mathbf{r}, \theta), \\ \left(\omega_n - \frac{v_F(\theta)}{2} \frac{d}{dr_{\parallel}}\right) f^{\dagger}(i\omega_n, \mathbf{r}, \theta) &= \Delta^*(\mathbf{r}, \theta) g(i\omega_n, \mathbf{r}, \theta), \\ v_F(\theta) \frac{d}{dr_{\parallel}} g(i\omega_n, \mathbf{r}, \theta) &= \Delta^*(\mathbf{r}, \theta) f(i\omega_n, \mathbf{r}, \theta) \\ &\quad - \Delta(\mathbf{r}, \theta) f^{\dagger}(i\omega_n, \mathbf{r}, \theta), \end{aligned} \quad (2.4)$$

which are supplemented by

$$\begin{aligned} g(i\omega_n, \mathbf{r}, \theta) &= [1 - f(i\omega_n, \mathbf{r}, \theta) f^{\dagger}(i\omega_n, \mathbf{r}, \theta)]^{1/2}, \\ \text{Re } g(i\omega_n, \mathbf{r}, \theta) &> 0. \end{aligned} \quad (2.5)$$

Here, $\bar{\mathbf{k}} = (\cos \theta, \sin \theta)$,

$$\begin{aligned} \mathbf{v}_F(\bar{\mathbf{k}}) &= (|\mathbf{v}_F(\theta)| \cos \Theta(\theta), |\mathbf{v}_F(\theta)| \sin \Theta(\theta)) \\ &= (v_F(\theta) \cos \Theta(\theta), v_F(\theta) \sin \Theta(\theta)), \end{aligned} \quad (2.6)$$

and the following coordinate system is taken: $\bar{\mathbf{u}} = \cos \Theta \bar{\mathbf{x}} + \sin \Theta \bar{\mathbf{y}}$, $\bar{\mathbf{v}} = -\sin \Theta \bar{\mathbf{x}} + \cos \Theta \bar{\mathbf{y}}$, and thus a point $\mathbf{r} = x\bar{\mathbf{x}} + y\bar{\mathbf{y}}$ is denoted as $\mathbf{r} = r_{\parallel} \bar{\mathbf{u}} + r_{\perp} \bar{\mathbf{v}}$. The center of a vortex line is situated at the origin $\mathbf{r} = (0, 0)$. The angle θ , i.e., the direction of $\bar{\mathbf{k}}$ is measured from the a axis (or x axis) in the hexagonal plane of NbSe₂. If one considers a cylindrical Fermi surface with anisotropic Fermi velocity, then $\mathbf{v}_F(\bar{\mathbf{k}}) = v_F(\theta) \bar{\mathbf{k}} = (v_F(\theta) \cos \theta, v_F(\theta) \sin \theta)$.

The self-consistent equation is given by

$$\Delta(\mathbf{r}, \theta) = N_0 2\pi T \sum_{\omega_n > 0} \int_0^{2\pi} \frac{d\theta'}{2\pi} \rho(\theta') V(\theta, \theta') f(i\omega_n, \mathbf{r}, \theta'), \quad (2.7)$$

where N_0 is the total density of states over the Fermi surface in the normal state. The θ -dependence of the density of states at the Fermi surface is represented by

$$\rho(\theta) = \frac{k_F(\bar{\mathbf{k}})}{N_0 |\bar{\mathbf{k}} \cdot \mathbf{v}_F(\bar{\mathbf{k}})|}, \quad (2.8)$$

which satisfies $\int (d\theta/2\pi) \rho(\theta) = 1$. We assume that the pairing interaction $V(\theta, \theta')$ is separable, i.e., $V(\theta, \theta') = vF(\theta)F(\theta')$, where v is the strength of the pairing interaction and $F(\theta)$ is a symmetry function, e.g., $F(\theta) = \cos 2\theta$ for a d -wave pairing, $F(\theta) = 1$ for an isotropic s -wave pairing, etc.

The pair potential is written as

$$\Delta(\mathbf{r}, \theta) = \Delta(\mathbf{r}) F(\theta). \quad (2.9)$$

To obtain a self-consistent pair potential, we solve Eqs. (2.4) and (2.7) iteratively. This computation is performed after a method of Ref. [39]. In the calculation of the pair potential, we adopt the so-called explosion method[49, 50] to solve Eq. (2.4).

The LDOS is evaluated from

$$\begin{aligned} N(E, \mathbf{r}) &= N_0 \int_0^{2\pi} \frac{d\theta}{2\pi} \rho(\theta) \text{Re } g(i\omega_n \rightarrow E + i\eta, \mathbf{r}, \theta) \\ &\equiv \int_0^{2\pi} \frac{d\theta}{2\pi} \rho(\theta) N(E, \mathbf{r}, \theta), \end{aligned} \quad (2.10)$$

where η (>0) is a small real constant. The value of η represents the effect of dilute impurities in a rough approximation[31, 33] or other smearing effects[51]. To obtain $g(i\omega_n \rightarrow E + i\eta, \mathbf{r}, \theta)$, we have to solve Eq. (2.4) for $\eta - iE$ instead of the Matsubara frequency ω_n . While we succeeded in this calculation in the vortex lattice case with the explosion method, a huge computer-running-time for the numerical calculation was needed in this method[42]. In the case of the isolated single vortex, however, it is convenient to utilize a method of the Riccati equation developed by Schopohl[34, 35, 52]. The Riccati equation simplifies the numerical computation.

The Riccati equations[34] are given as

$$v_F(\theta) \frac{d}{dr_{\parallel}} a(\omega_n, \mathbf{r}, \theta) - \Delta(\mathbf{r}, \theta) + \left(2\omega_n + \Delta^*(\mathbf{r}, \theta) a(\omega_n, \mathbf{r}, \theta) \right) a(\omega_n, \mathbf{r}, \theta) = 0, \quad (2.11)$$

$$v_F(\theta) \frac{d}{dr_{\parallel}} b(\omega_n, \mathbf{r}, \theta) + \Delta^*(\mathbf{r}, \theta) - \left(2\omega_n + \Delta(\mathbf{r}, \theta) b(\omega_n, \mathbf{r}, \theta) \right) b(\omega_n, \mathbf{r}, \theta) = 0. \quad (2.12)$$

Equations (2.11) and (2.12) are obtained by substituting the following parametrization[34] into the Eilenberger equations (2.4),

$$f = \frac{2a}{1+ab}, \quad f^\dagger = \frac{2b}{1+ab}, \quad g = \frac{1-ab}{1+ab}. \quad (2.13)$$

We solve Eqs. (2.11) and (2.12) independently along the r_{\parallel} trajectory where r_{\perp} is held constant. In the isolated single vortex under consideration, one can integrate Eqs. (2.11) and (2.12) using solutions far from the vortex,

$$\begin{aligned} a_{-\infty} &= \frac{\sqrt{\omega_n^2 + |\Delta(-\infty, r_{\perp}, \theta)|^2} - \omega_n}{\Delta^*(-\infty, r_{\perp}, \theta)}, \\ b_{+\infty} &= \frac{\sqrt{\omega_n^2 + |\Delta(+\infty, r_{\perp}, \theta)|^2} - \omega_n}{\Delta(+\infty, r_{\perp}, \theta)} \quad (\omega_n > 0) \end{aligned} \quad (2.14)$$

as the initial values, respectively[52]. To obtain stable solutions, the integral for a is performed from $r_{\parallel} = -\infty$, and for b from $r_{\parallel} = +\infty$ [52]. We numerically integrate the first-order differential equations (2.11) and (2.12) by the adaptive stepsize control Runge-Kutta method[53]. The Green's function $g(i\omega_n \rightarrow E + i\eta, \mathbf{r}, \theta)$ is obtained from Eq. (2.13) if one solves Eqs. (2.11) and (2.12) for $\eta - iE$ instead of ω_n . When we solve Eqs. (2.11) and (2.12) for $\eta - iE$, we use the self-consistently obtained pair potential $\Delta(\mathbf{r})$ which is calculated beforehand.

From now on (in this chapter), the density of states, energies, and lengths are measured in units of N_0 , the uniform gap Δ_0 at the temperature $T = 0$, and the coherence length $\xi_0 = v_{F0}/\Delta_0$ ($v_{F0} \equiv k_F/N_0$), respectively.

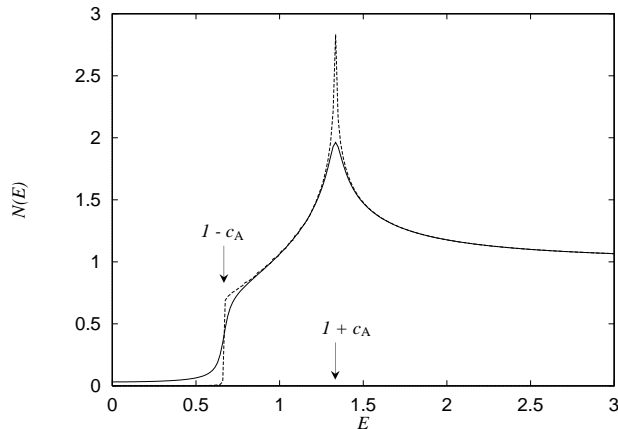


Figure 2.1: The density of states $N(E)$ at zero field, where smearing parameter $\eta = 0.03$ (solid line) or $\eta = 0.001$ (dashed line). It is calculated for the isotropic cylindrical Fermi surface, and the degree of the gap anisotropy is $c_A = 1/3$.

2.3 Pair potential and local density of states

Before going into technical details, we briefly explain our model and its parameter involved in connection with NbSe₂, which is a typical type-II *s*-wave superconductor. We assume the following model of an anisotropic *s*-wave pairing in Eq. (2.9),

$$F(\theta) = 1 + c_A \cos 6\theta. \quad (2.15)$$

Here we again stress that the angle θ , i.e., the direction of $\bar{\mathbf{k}}$ is measured from the *a* axis (or *x* axis) in the hexagonal plane of NbSe₂. Thus the parameter c_A denotes the degree of anisotropy in the superconducting energy gap[54, 55, 56]. The case $c_A = 0$ corresponds to a conventional isotropic gap.

The anisotropic *s*-wave gap is certainly suggested in NbSe₂ from a scanning tunneling spectroscopy (STS) experiment at zero field[15]. The *I*-*V* tunneling spectrum, observed at the extreme low temperature $T = 50$ mK, indicates a substantial gap anisotropy (the gap amplitude with the averaged value 1.1 meV distributes from 0.7 to 1.4 meV, see Fig. 1 in Ref. [15]), which is consistent with the density of states in the anisotropic *s*-wave gap case [Fig. 2.1]. It is seen from Fig. 2.1 that the gap edge distributes from $E = 1 - c_A$ to $1 + c_A$ in the case of the anisotropic gap. Then, the experimental data of STS[15] indicate that $c_A \sim 1/3$. Similarly, a nuclear quadrupole resonance, NQR, experiment[57] in NbSe₂ suggests an anisotropic *s*-wave energy gap. The temperature dependence of the spin-lattice relaxation rate $1/T_1$ is well fitted by an anisotropic energy gap model following Hebel[58] with the value of a parameter $\delta/\Delta(0) \sim 1/3$ [57]. Here the broadening in the gap edge, $\delta/\Delta(0)$, of Ref. [57] corresponds to $\delta/\eta_0(0)$ of Ref. [58]. This parameter $\delta/\Delta(0)$ corresponds well to our parameter of the gap anisotropy, c_A , because both parameters δ and c_A yield the broadening in the gap edge. We set $c_A = 1/3$ as a representative case in the following.

In this chapter, we restrict our attention to the gap anisotropy effect only, neglecting other effects, i.e., the vortex lattice effect and the effect of the

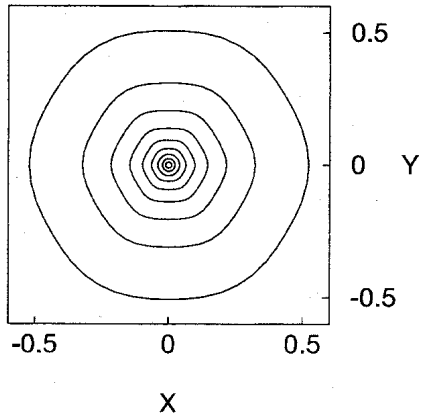


Figure 2.2: Contour plot of the amplitude of the real-space variation part of the pair potential, $|\Delta(\mathbf{r})|$. From the center, 0.1, 0.2, \dots , 0.9. The temperature is $T = 0.1T_c$, and the degree of the gap anisotropy is $c_A = 1/3$.

anisotropic density of states at the Fermi surface, to clearly see how the energy gap anisotropy influences the LDOS. We calculate the LDOS in the isolated vortex case assuming an isotropic cylindrical Fermi surface ($\mathbf{v}_F(\mathbf{k}) \parallel \mathbf{k}$, $v_F(\theta) = v_{F0}$).

2.3.1 Pair potential

In order to calculate the LDOS, we need the self-consistent pair potential obtained at the temperature, say, $T = 0.1T_c$ (T_c is the superconducting transition temperature). The self-consistently obtained real-space variation part of the pair potential, $\Delta(\mathbf{r})$, certainly exhibits a weak sixfold structure both in its phase and amplitude, which results from the anisotropic pairing, Eq. (2.15). This behavior is similar to that of the d -wave case[39], but sixfold symmetric here. In Fig. 2.2, we show a contour plot of the amplitude of $\Delta(\mathbf{r})$. The amplitude $|\Delta(\mathbf{r})|$ is slightly suppressed in the x axis direction and its equivalent directions. As shown in Fig. 2.2, the spatial variation of $\Delta(\mathbf{r})$ has weak anisotropy, but is almost circularly symmetric. However, the LDOS shows the characteristic sixfold symmetric structure as mentioned below.

2.3.2 Local density of states

The LDOS calculated using the self-consistent pair potential has almost the same structure, except for the length scale for its spread, as that calculated using a test-potential $\Delta(\mathbf{r}) = \Delta(T) \tanh(r/\xi) \exp(i\phi)$ does, where $\Delta(T)$ is the uniform gap at the temperature T , $\xi = v_{F0}/\Delta(T)$, and the cylindrical coordinate system $\mathbf{r} = (r, \phi)$ is taken. That is, the LDOS does not so affected by the weak sixfold symmetric spatial structure of the real-space variation part of the pair potential, $\Delta(\mathbf{r})$. We have seen the same situation also in the d -wave case.[39] It means that a calculated sixfold or fourfold structure of the LDOS directly

results from the k -space variation part of the pair potential, $F(\theta)$.

In Fig. 2.3, we show the LDOS $N(E, r)$ for several energies E in the case $c_A = 1/3$, calculated by using the self-consistently obtained pair potential. It is seen from Fig. 2.3(a) that the sixfold star centered at the vortex center is oriented away from the x axis by 30° for $E = 0$. Next it is seen from Fig. 2.3(b) that at the intermediate energy each ray splits into two parallel rays, keeping its direction. This characteristic feature was precisely observed in the experiment by Hess[13, 14]. With increasing the energy E further, the sixfold star becomes a more extended one, and its orientation rotates by 30° as seen from Fig. 2.3(c). Note that in Fig. 2.3(c) the head of each ray splits in two. It coincides with an experimental result (see the STM image for 0.48 mV in Fig. 1 of Ref. [13]). In this way, the anisotropic s -wave gap model well reproduces the experimental features mentioned in Sec. 2.1: (1) the sixfold star shape, (2) the 30° rotation, and especially (3) the split parallel ray structure at the intermediate energy. We refer to Fig. 1 in Ref. [41] [Fig. 2.4 in this thesis] where the density plots of the LDOS compared with the experimental data are displayed, which is complimentary to Fig. 2.3 in the present chapter.

Another way to examine the quasiparticle excitations in the vortex states is to see how the spectrum evolves along radial lines from the vortex center. We show the spectral evolutions along the radial lines for 30° in Fig. 2.5(a), 15° in 2.5(b), and 0° in 2.5(c) from the x axis. The zero-bias peak splits into several peaks in each spectral evolution. Cross sections of each spectral evolution at $r = 1$ ($r = \sqrt{x^2 + y^2}$) are shown in Fig. 2.6 to provide the identification of each ridge in Fig. 2.5.

In the calculation of Figs. 2.3 and 2.5, the smearing factor is chosen as $\eta = 0.03$, which well reproduces the STM experimental data. It corresponds to the solid lines of Fig. 2.6, where the peaks are labeled α - ε . The case with smaller smearing effect ($\eta = 0.001$) is represented by the dashed lines in Fig. 2.6, where the spectrum has the sharp peaks labeled as A-E. (The structure of these peaks is discussed in the next section.) As shown in Fig. 2.6, by increasing the smearing effect, the spectrum of the dashed line ($\eta = 0.001$) is reduced to that of the solid line ($\eta = 0.03$), and reproduces the STM experimental data. It seems that the LDOS actually observed in STM experiments is somewhat smeared due to impurities[31, 33] or other smearing effects[51].

In Fig. 2.5(a) (the 30° direction), there exist one peak at $E = 0$ and three pairs of peaks. The peak at $E = 0$ in Fig. 2.5(a) [the ε peak in Fig. 2.6(a)] corresponds to the ray which extends in the 30° direction in Fig. 2.3(a). This peak is referred to as the inner peak in Refs. [8] and [15]. This inner peak [the ε peak] corresponds to also the split parallel ray in Fig. 2.3(b) and the head of the ray which splits into two in Fig. 2.3(c). The inner ε peak is, therefore, sensitive to the angle of the radial line, and splits in a pair of peaks with the variation of the angle [see Figs. 2.5(b) and 2.5(c)]. On the other hand, the most inside pair of peaks in Fig. 2.5(a) [the δ peak in Figs. 2.5 and 2.6] is not sensitive to the angle. This peak is referred to as the outer peak[8, 15]. As shown in Fig. 2.7, the behavior of the calculated inner and outer peaks well coincide with the experimental result (the experimental feature (4) in Sec. 2.1). The positions of the outer δ and inner ε peaks as a function of r are compared with the experimental data in Fig. 3 of Ref. [41] [Fig. 2.9].

Outside the inner ε and outer δ peaks, extra peaks appear in each calculated spectral evolution [the α , β , and γ peaks in Figs. 2.5 and 2.6]. The result of

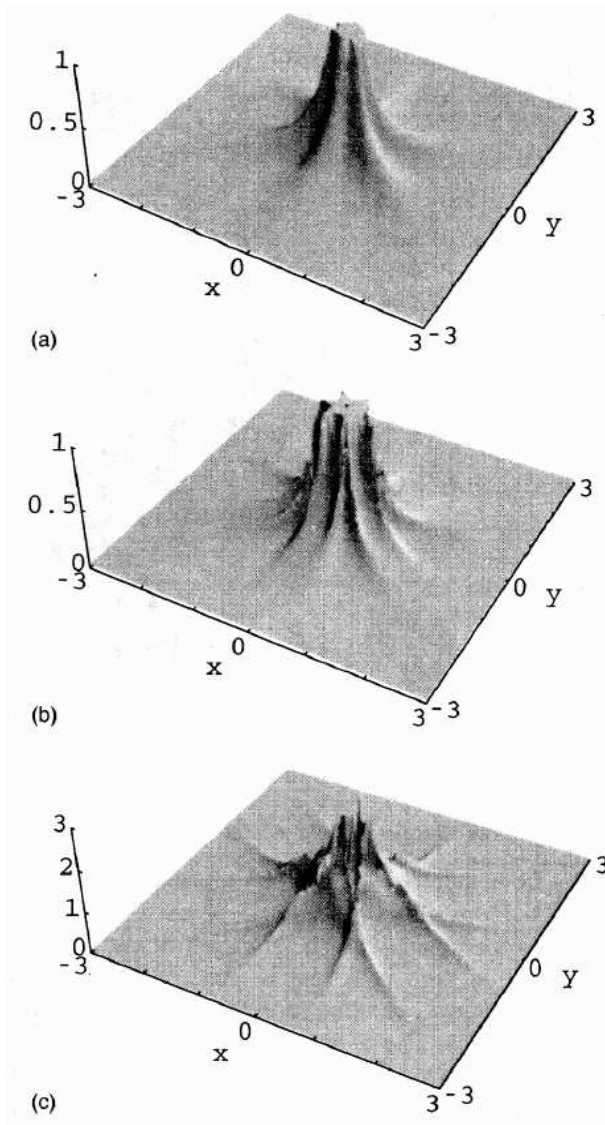


Figure 2.3: The LDOS $N(E, \mathbf{r})$ ($\eta = 0.03$) calculated for the energies $E = 0$ (a), 0.2 (b), and 0.4 (c). Large peaks in the vicinity of the vortex center are truncated in the figures (a) and (b).

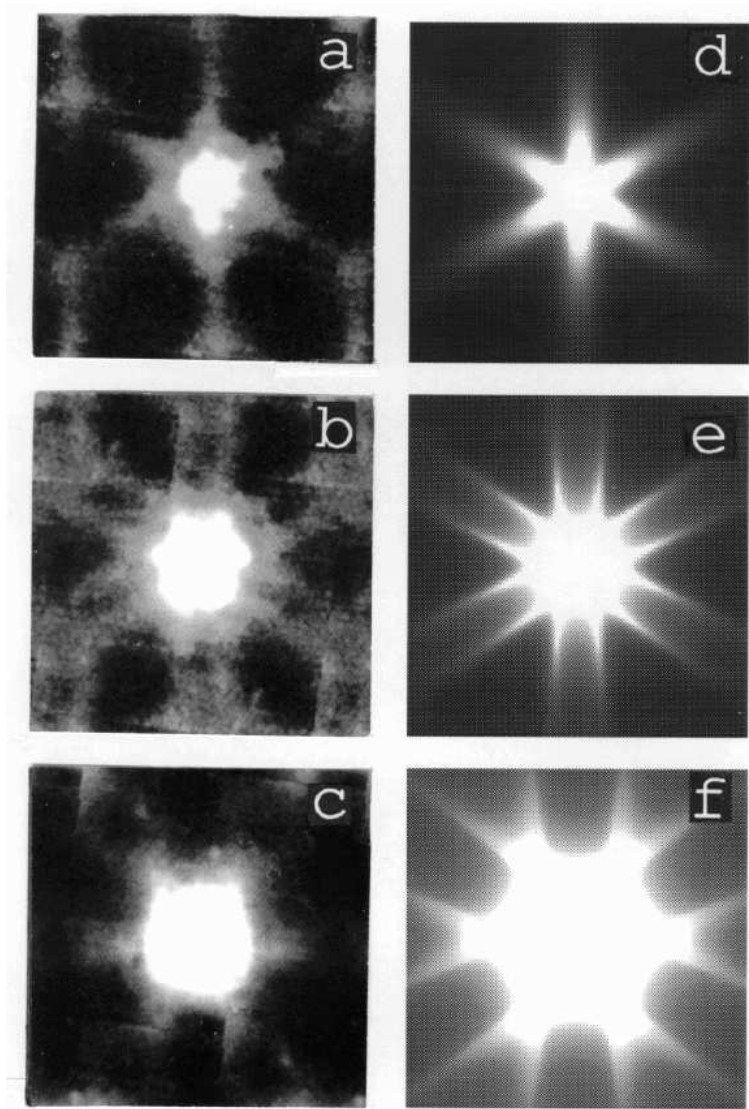


Figure 2.4: *Left column:* Tunneling conductance images observed by Hess *et al.* at 0.1 Tesla for the bias voltage 0.0mV (a), 0.24mV (b), 0.48mV (c), where $1759\text{\AA} \times 1759\text{\AA}$ is shown (also see Refs. [13] and [14]). The horizontal direction is the nearest-neighbor direction of the vortex lattice and also is the crystallographic \mathbf{a} direction in NbSe₂. *Right column:* The LDOS images calculated for $E = 0$ (d), 0.2 (e), and 0.32 (f), where $6\xi_0 \times 6\xi_0$ is shown and $c_A = 1/2$.

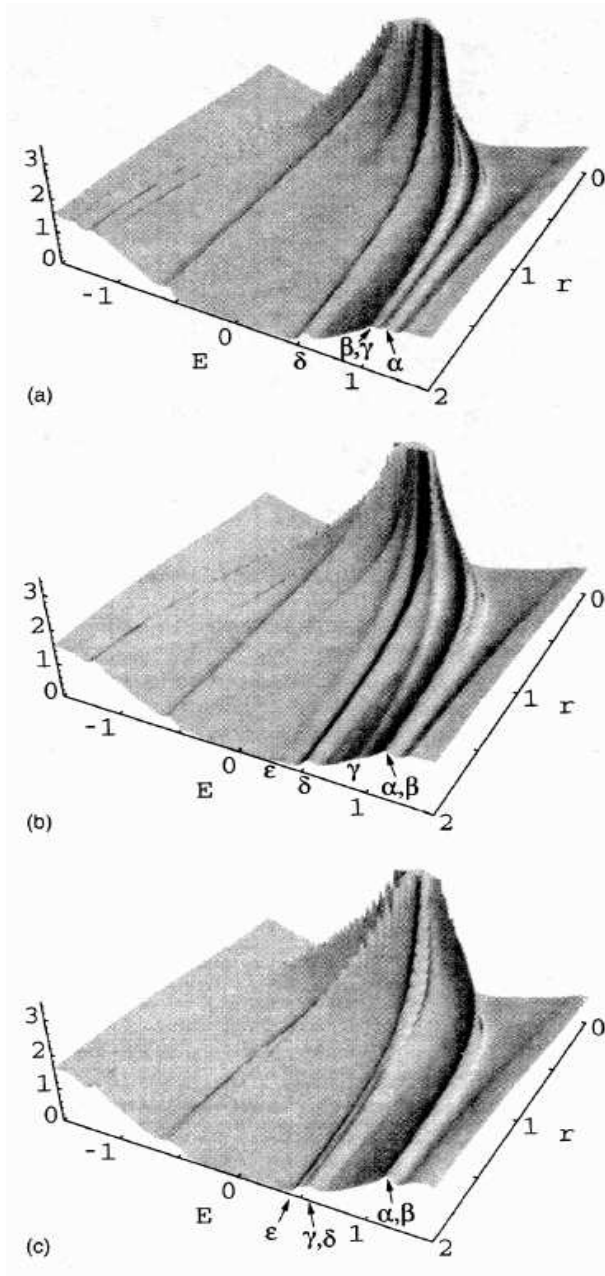


Figure 2.5: Spectral evolutions $N(E, r)$ ($\eta = 0.03$) along radial lines for 30° (a), 15° (b), and 0° (c) from the x axis. The zero-bias peak is truncated in the figures. The peak lines in the spectra are labeled α - ϵ .

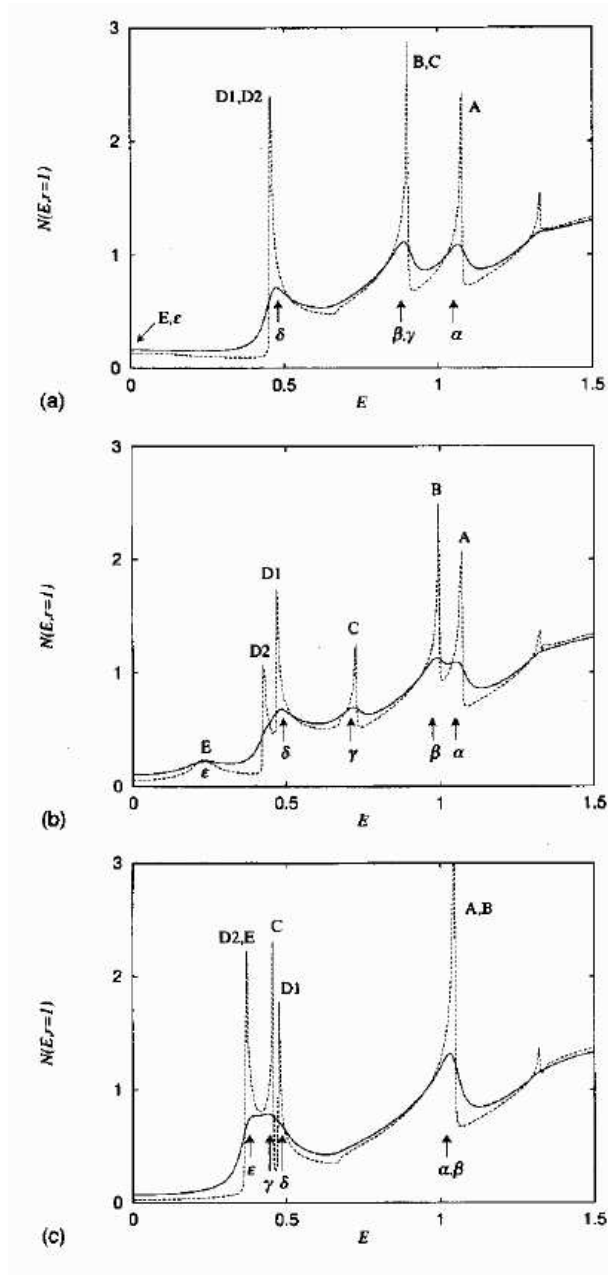


Figure 2.6: Cross sections of the spectral evolutions (Fig. 2.5) at the distance from the vortex center, $r = 1$. The directions of each radial line are 30° (a), 15° (b), and 0° (c) from the x axis. The peaks in the spectra are labeled A–E for the dashed line spectra ($\eta = 0.001$) and α – ϵ for the solid line spectra ($\eta = 0.03$). The labels α – ϵ correspond to those of Fig. 2.5.

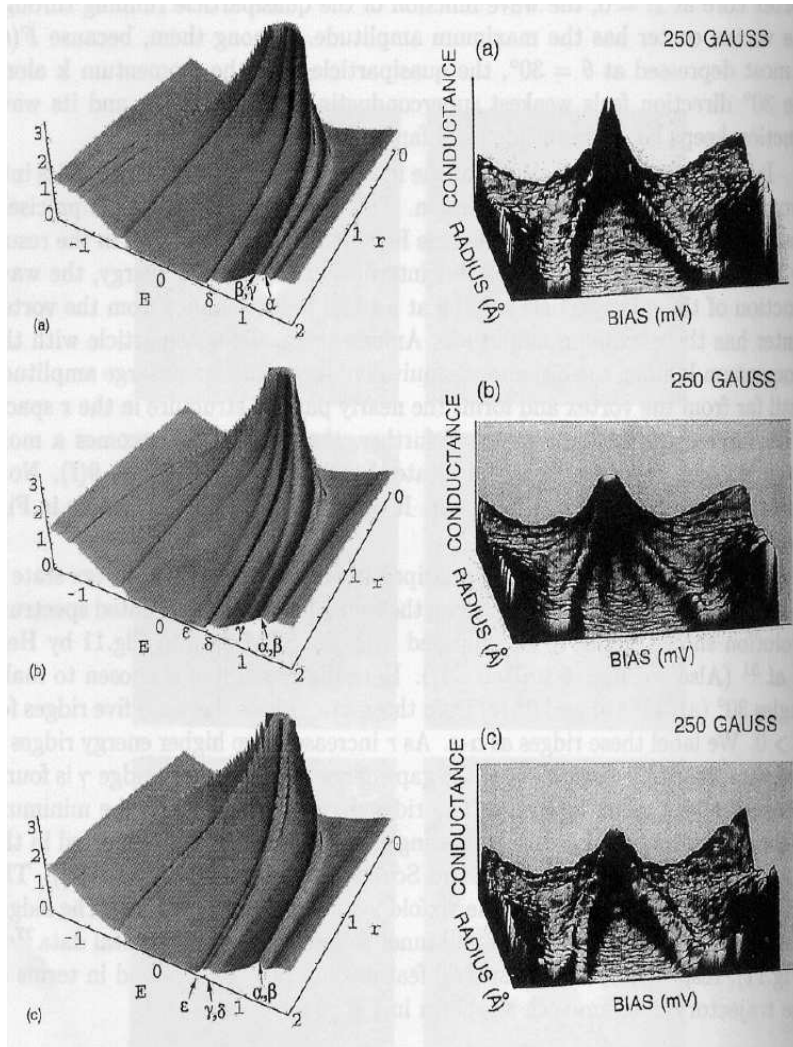


Figure 2.7: Comparison of the spectral evolutions between the theory and experiment. *Left column:* The theoretically calculated spectral evolutions $N(E, r)$ ($\eta = 0.03$) along radial lines for 30° (a), 15° (b), and 0° (c) from the x axis [Fig. 2.5]. *Right column:* The experimentally observed tunneling conductance $dI/dV(V, r)$ on NbSe₂ (from Ref. [8]), 30° (a), 15° (b), and 0° (c) from the a axis [Fig. 1.5]. Note that there exists nice coincidence on the behavior of the (inner and outer) peaks.

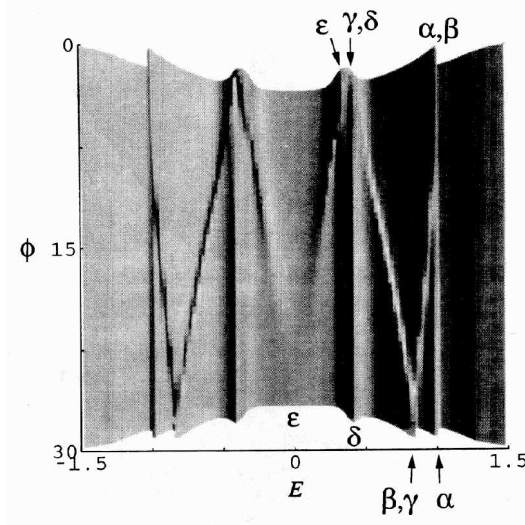


Figure 2.8: Spectral evolution $N(E, \mathbf{r})$ ($\eta = 0.03$) from the angle 0° to 30° along a circle whose radius $r = 1$. The center of this circle is situated at the vortex center. The peaks labeled as α - ε correspond to those of Figs. 2.5 and 2.6.

the calculation shows that the extra peaks are relatively sensitive to the angle of the radial line. The existence of the extra peaks is characteristic of the gap anisotropy effect. The peaks α and β merge into the upper edge of the energy gap, $1 + c_A$, far from the vortex. These extra peaks have not been noted in experimental data so far. While each peak cannot be clearly identified in experimental data yet, it seems that there is at least one new line outside the outer peak in the data[59]. It is expected for future experiments to definitely identify the extra peaks.

The dependence of the LDOS on the angle of the radial line is important, because it gives a detailed information on the gap anisotropy. To see it, we show in Fig. 2.8 a spectral evolution from the angle 0° to 30° along a circle whose radius $r = 1$. From this, we can see how each peak moves, and joins up the others with the variation of the angle. As mentioned above, the ε peak (that is, inner peak) is sensitive to the angle ϕ of the radial line, and the δ peak (outer peak) is insensitive to ϕ . The ε peak is located at $E = 0$ for $\phi = 30^\circ$. When ϕ deviates from 30° , the peak splits into two which are positive and negative energy peaks. With decreasing ϕ to 0° , the energy E -position of the ε peak increases. As for the peaks α , β , and γ , with decreasing ϕ from 30° to 0° , the E -position decreases for the γ peak, increases for the β peak, and is insensitive for the α peak. The peaks β and γ overlap each other for $\phi = 30^\circ$, and the peaks α and β overlap each other for $\phi = 0^\circ$ (see also Fig. 2.6). Here, we should mention the behavior of the γ peak at $\phi \sim 0^\circ$. In Fig. 2.8, the γ peak seems to join up the angle-insensitive δ peak near 0° , that is, the γ peak is buried in the δ peak in Figs. 2.5(c) and 2.6(c) (the 0° direction). Such a behavior of the γ peak intimately relates to the value of the anisotropic gap parameter, c_A . The above behavior of γ is that of the case $c_A = 1/3$. According as c_A increases

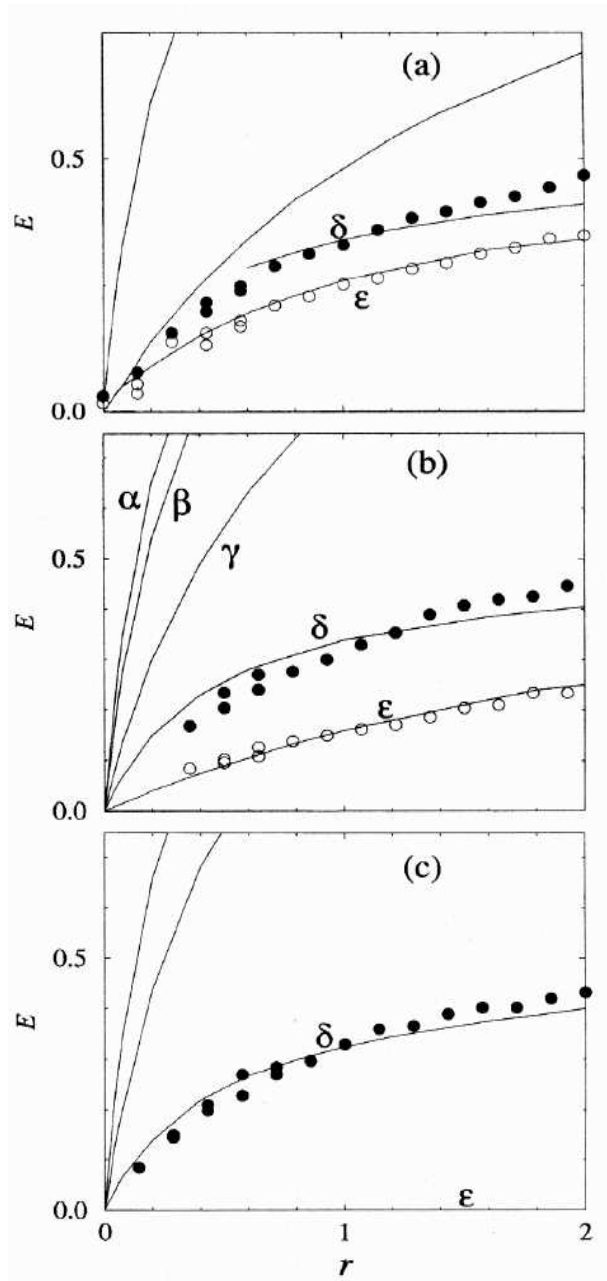


Figure 2.9: The ridge energies of the LDOS as a function of r along the radial lines for 0° (a), 15° (b), and 30° (c) from the x axis (solid lines). $c_A = 1/2$. The labels α - ϵ are the same as those in Fig. 2.5. Experimental data (Ref. [15]) are also presented by points \bullet (outer) and \circ (inner), where r and E are scaled by 350\AA and 1.67mV , respectively.

further, the position of the γ peak at 0° shifts to the higher energy side [see a spectral evolution shown in Fig. 3(a) of Ref. [41] (the 0° direction) [Fig. 2.9(a) in this thesis], where c_A is set to $1/2$ and we can see that a peak line, which corresponds to the present peak γ (not denoted explicitly in that figure), evolves away from the δ peak line].

2.4 Quasiparticle trajectories

In this section, we interpret the behavior of the quasiparticle bounded around a vortex in terms of the quasiclassical picture.

2.4.1 Direction-dependent local density of states

In the quasiclassical approximation, the equations are independently given for each direction of $\bar{\mathbf{k}}$. The Eilenberger equation (or the Riccati equation) for a direction $\bar{\mathbf{k}}$ is independent of those for the other directions. The direction-dependent local density of states $N(E, \mathbf{r}, \theta)$ introduced in Eq. (2.10) is obtained from the solution of the equation for the direction $\bar{\mathbf{k}} = (\cos \theta, \sin \theta)$. The LDOS $N(E, \mathbf{r})$ is calculated by integrating the direction-dependent LDOS $N(E, \mathbf{r}, \theta)$ over θ . In an isolated vortex state, the structure of $N(E, \mathbf{r}, \theta)$ was previously investigated analytically[22, 30, 32] and numerically[30]. According to the results of these investigations, $N(E, \mathbf{r}, \theta)$ has the following structure for low energies below Δ_0 in the isolated single vortex[22, 30, 32]. (Here, remind ourselves of the notation: $\mathbf{r} = x\bar{\mathbf{x}} + y\bar{\mathbf{y}} = r_{\parallel}\bar{\mathbf{u}} + r_{\perp}\bar{\mathbf{v}}$; $\bar{\mathbf{u}} = \cos \theta\bar{\mathbf{x}} + \sin \theta\bar{\mathbf{y}}$, $\bar{\mathbf{v}} = -\sin \theta\bar{\mathbf{x}} + \cos \theta\bar{\mathbf{y}}$.) (i) $N(E, \mathbf{r}, \theta)$ as a function of $\mathbf{r} = (r_{\parallel}, r_{\perp})$ vanishes everywhere except on a straight line along which $r_{\perp} = \text{const.} = r_{\perp}(E)$. This straight line and $r_{\perp}(E)$ are referred to as “quasiparticle path” and “impact parameter,” respectively. (ii) Along the line $r_{\perp} = r_{\perp}(E)$, $N(E, \mathbf{r}, \theta)$ has a single maximum at $r_{\parallel} = 0$ and decreases exponentially for $r_{\parallel} \rightarrow \pm\infty$. (iii) The impact parameter $r_{\perp}(E)$ is a monotonically increasing function of E . One defines $E(r_{\perp})$ as the energy level of the state on the quasiparticle path with the impact parameter r_{\perp} . In extreme type-II superconductors where $\kappa \gg 1$, $E(r_{\perp})$ is determined by the minimum value of the amplitude of the pair potential on the quasiparticle path $r_{\perp} = r_{\perp}(E)$. For the low energy levels, $E(r_{\perp})$ is given by $E(r_{\perp}) = \text{sgn}(r_{\perp})|\Delta(r_{\parallel} = 0, r_{\perp})|$ in a good approximation.

On the basis of the above properties (i)–(iii) of the direction-dependent LDOS $N(E, \mathbf{r}, \theta)$ studied by Kramer and Pesch[22], Klein[30], and Ullah *et al.*[32], we interpret our result of the preceding section as follows.

For simplicity, we concentrate our attention to Eq. (2.11) as a representative. Dividing Eq. (2.11) by $F(\theta)$, we rewrite this equation as

$$\frac{1}{F(\theta)} \frac{d}{dr_{\parallel}} a(\omega_n, \mathbf{r}, \theta) - \Delta(\mathbf{r}) + \left(2 \frac{\omega_n}{F(\theta)} + \Delta^*(\mathbf{r}) \right) a(\omega_n, \mathbf{r}, \theta) = 0. \quad (2.16)$$

In the case of the isotropic s -wave pairing ($F(\theta) = 1$), $N(E, \mathbf{r}, \theta)$ at a fixed energy has the identical structure for each direction θ [the items (i), (ii), and (iii)]. Then the LDOS $N(E, \mathbf{r})$, obtained by integrating $N(E, \mathbf{r}, \theta)$ over θ , exhibits a “ring” shaped structure[34] in the real space. The impact parameter is the radius of the ring.

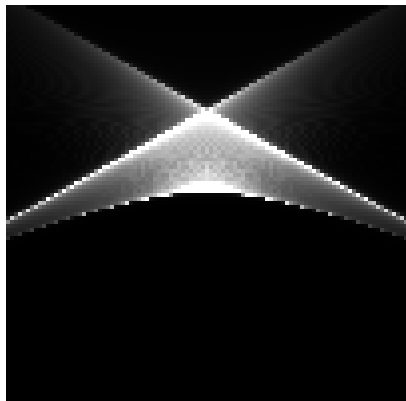


Figure 2.10: The direction-dependent LDOS $N(E, \mathbf{r}, \theta)$ partly integrated from $\theta = -30^\circ$ to 30° , where $E = 0.5$, $\eta = 0.001$, and $6\xi_0 \times 6\xi_0$ is shown in the real space.

In the case of an anisotropic pairing, the situation is changed because of the terms which include $F(\theta)$ in Eq. (2.16). According to Eq. (2.16), both the length scale in the r_{\parallel} direction and the energy scale vary with θ , but otherwise the form of the equation is same as that of the isotropic s -wave case. For the direction θ where $F(\theta)$ is suppressed, the length of the spreading of $N(E, \mathbf{r}, \theta)$ along the quasiparticle path becomes large [note the items (i) and (ii), and the term $\frac{1}{F(\theta)} \frac{da}{dr_{\parallel}}$ in Eq. (2.16)]. For the same θ , the effective energy becomes large and then the impact parameter becomes far from the vortex center [note the item (iii) and the term $2\frac{\omega_n}{F(\theta)}a$ in Eq. (2.16)].

2.4.2 Interpretation on the LDOS around a vortex

We show the partly integrated $N(E, \mathbf{r}, \theta)$ in Fig. 2.10, where the integration is done from $\theta = -30^\circ$ to 30° , and its schematic figure in Fig. 2.11, for the pairing of Eq. (2.15) where $c_A = 1/3$. Here, to clarify the structure of the LDOS, a small smearing parameter ($\eta = 0.001$) is adopted. The peak lines shown in Fig. 2.10 are composed of the quasiparticle paths of each direction θ described above. These peak lines can be interpreted as the flows of quasiparticles shown in Fig. 2.11. It is noted that the trajectories 1 and 2 appear, because $F(\theta)$ is finite at $\theta = -30^\circ$ and 30° , i.e., the impact parameter is finite at these angles. If $F(\theta)$ has a node, i.e., $c_A = 1$, the impact parameter is infinitely far from the vortex center for the quasiparticle path of the node direction[60], and the trajectories 1 and 2 disappear. In the bound states, the quasiparticles flow along these trajectories. We call it “quasiparticle trajectory.” The whole state at a fixed energy is composed of such flows of quasiparticles along the quasiparticle trajectories, while the individual quasiparticle paths of each direction θ [the items (i) – (iii)] could be considered to be the Andreev reflections.

We show in Fig. 2.12 the LDOS $N(E, \mathbf{r})$ obtained by integrating the direction-dependent LDOS $N(E, \mathbf{r}, \theta)$ over all θ . A schematic figure which corresponds to Fig. 2.12 is shown in Fig. 2.13. The peaks which the radial lines cross are

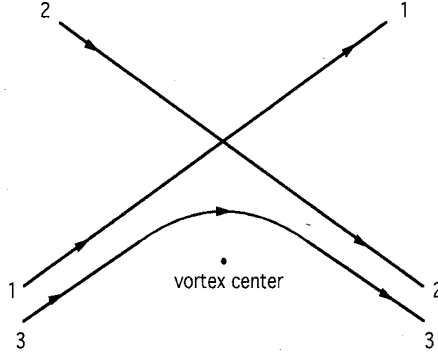


Figure 2.11: Schematic flow trajectories of quasiparticles with an energy $0 < E < (1 - c_A)$. These trajectories correspond to those shown in Fig. 2.10. When $(1 - c_A) < E < (1 + c_A)$, the trajectories 1 and 2 disappear and only the trajectory 3 is alive.

labeled A–E there. When the energy E elevates, the scale of the trajectory in Fig. 2.13 increases with keeping its structure fixed. Therefore, the trajectory has one-to-one correspondence to the peak of the spectrum of Figs. 2.5–2.8. The peaks A–E of Fig. 2.13 precisely correspond to those of Fig. 2.6. These peaks are smeared to appear as α - ε peaks in Fig. 2.6 (and thus in Figs. 2.5 and 2.8). The LDOS actually observed in STM experiments is not that shown in Fig. 2.12 itself, but somewhat smeared one [Figs. 2.3, 2.5, and 2.6] due to impurities[31, 33] or other smearing effects[51]. Roughly speaking, the peaks A, B, C, D1, and E correspond to the peaks α , β , γ , δ , and ε , respectively.

The trajectory of Fig. 2.13 helps us to facilitate an understanding of the rich structure of the LDOS. The trajectories B and C cross each other at the angle $\phi = 30^\circ$ from the x -axis in Fig. 2.13. Then, the peaks B and C (i.e., β and γ) overlap each other in Figs. 2.5(a) and 2.6(a). The cross of the trajectories A and B at $\phi = 0^\circ$ in Fig. 2.13 corresponds to the overlap of the peaks A and B (i.e., α and β) in Figs. 2.5(c) and 2.6(c). When ϕ varies from 30° to 0° , the trajectories C and D1 cross each other in Fig. 2.13, where $c_A = 1/3$. It corresponds to the result that the peaks γ and δ interchange their positions between Figs. 2.6(b) and 2.6(c). However, this behavior of γ and δ depends on the anisotropic gap parameter c_A as mentioned at the end of Sec. 2.3. In the case of large c_A , the trajectories C and D1 does not cross for $0^\circ \leq \phi \leq 30^\circ$ in Fig. 2.13. Even at $\phi = 0^\circ$, the trajectory D1 is located farther from the vortex center than the trajectory C, for large c_A . Then, the peak C (i.e., γ) is located at higher energy than the peak D1 (i.e., δ) in the spectrum of Figs. 2.6(c) and 2.8, for large c_A . As seen in Fig. 2.6, the peak D2 tends to be buried in the other peaks, due to the smearing effects. However, if the experiment is performed for the weak smearing case, the peak D2 should be observed as a small peak, which splits from the peak D1 (i.e., δ) at $\phi = 30^\circ$ and approaches the peak E (i.e., ε) with decreasing ϕ to 0° . This D2 peak seems to be easily observed for the angle region $0^\circ < \phi < 10^\circ$. We detect a small indication of the D2 peak for this angle region, if Fig. 2.8 is enlarged at $\phi \sim 0^\circ$. The trajectories D1 and E (i.e., δ and ε) corresponds to

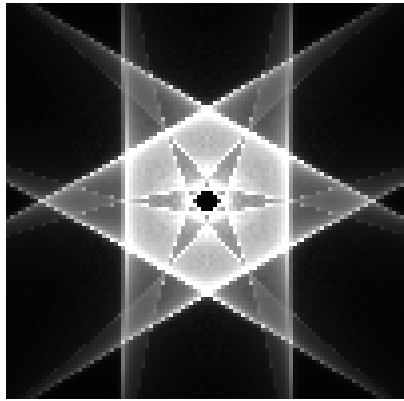


Figure 2.12: The LDOS $N(E, \mathbf{r})$ which is obtained by integrating the direction-dependent LDOS $N(E, \mathbf{r}, \theta)$ over θ , where $E = 0.5$, $\eta = 0.001$, and $6\xi_0 \times 6\xi_0$ is shown.

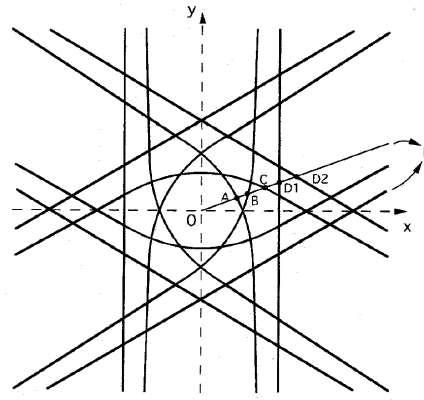


Figure 2.13: Schematic figure of the LDOS $N(E, \mathbf{r})$ for an energy $0 < E < (1 - c_A)$. Points A–E correspond to the peaks of the dashed line spectra in Fig. 2.6.

the trajectories 1 and 2 of Fig. 2.11, which is related to the lower edge of the anisotropic energy gap. Therefore, these trajectories disappear for the higher energy, $(1 - c_A) < E < (1 + c_A)$. The peaks D1 and E (i.e., δ and ε) merge into the lower edge of the energy gap at $E = 1 - c_A$ far from the vortex.

2.4.3 Flows of quasiparticles around a vortex

The flows of the quasiparticles mentioned above are quantitatively represented by the following quantity,

$$\mathbf{I}(E, \mathbf{r}) = \int_0^{2\pi} \frac{d\theta}{2\pi} \rho(\theta) \mathbf{v}_F(\theta) N(E, \mathbf{r}, \theta), \quad (2.17)$$

which we tentatively call “directional local density of states.” This directional LDOS corresponds to a quantity obtained by integrating “spectral current density” introduced by Rainer *et al.*[48] over θ (or \mathbf{p}_f in Ref. [48]). The total current density around a vortex is composed of the spectral current density[48]. In Figs. 2.14(a), 2.14(b), 2.14(c), and 2.14(d), we show the directional LDOS $\mathbf{I}(E, \mathbf{r})$ calculated for $E = 0.2, 1.2, 1.4,$ and $1.6,$ respectively. Here $\mathbf{I}(E, \mathbf{r})$ is calculated under the condition considered in this section, i.e., under the anisotropic gap and the isotropic cylindrical Fermi surface. It is seen from Fig. 2.14(a) that the flow of the quasiparticle exhibits a sixfold anisotropy resulting from the sixfold LDOS of the bound states (Fig. 2.3(b) and thus Fig. 2.13). Now, it is of interest to note the flow with an energy near the upper gap edge, $E = 1 + c_A$ ($\simeq 1.3$). Comparing Figs. 2.14(b) and 2.14(d), we can see that the quasiparticles above and below the upper gap edge flow each other in reverse directions except in the vicinity of the vortex center. It certainly coincides with a result of an analysis based on the Bogoliubov-de Gennes equation[16]. This feature should not be influenced by the gap anisotropy.

2.5 Summary and discussions

The LDOS around an isolated single vortex is studied within the framework of the quasiclassical theory. We consider the effect of the anisotropy of the superconducting energy gap. Assuming the anisotropic s -wave energy gap in Eq. (2.15), we succeed in theoretically reproducing the characteristic structure of the LDOS observed in STM experiments; the observed features, i.e., the items (1)–(4) for NbSe₂ listed in Sec. 2.1, are well described in terms of the anisotropic gap model. We point out the existence of the missing peaks (α , β , and γ) at the higher energy side in the spectral evolution shown in Figs. 2.5–2.8, which is expected to be looked for in a future experiment. We also notice the further splitting of the observed broad peaks as shown, for example, in Fig. 5(b) ($\delta \rightarrow$ D1 and D2). These predictions, which reflect the gap anisotropy, may be checked by using a purer sample at lower temperatures, because smearing effects, due to lattice defects or thermal broadening, mask the fine details. We attempt to interpret the calculated LDOS in terms of the quasiparticle trajectory. This enables us to thoroughly understand the STM results and the internal electronic structure of the vortex. In this chapter, the value of our parameter is chosen appropriate for NbSe₂. However, the essence of the obtained results should be applicable to other type-II superconductors in general although the degree

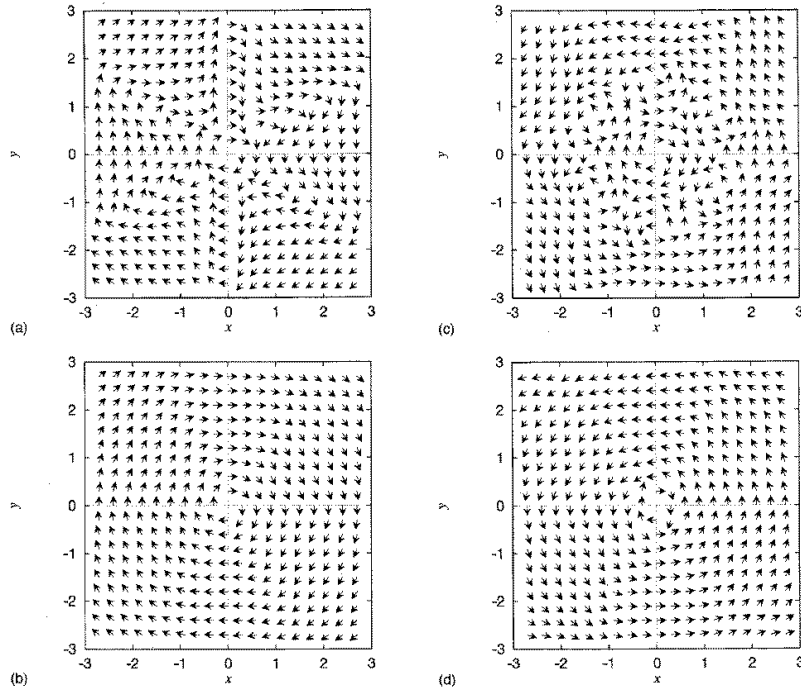


Figure 2.14: The directional LDOS $I(E, \mathbf{r})$ ($\eta = 0.03$) for the energies $E = 0.2$ (a), 1.2 (b), 1.4 (c), and 1.6 (d). The arrows in the figures represent only the directions of $I(E, \mathbf{r})$.

of the gap anisotropy c_A and the symmetry of $F(\theta)$ will be different in each case. Even in other anisotropic superconductors, the explanation in terms of the quasiparticle trajectory would be helpful to an understanding of the internal electronic structure of vortices.

2.5.1 Comparison with other theories and effects of the vortex lattice

Let us comment on prior works which are connected with the star-shaped LDOS observed in NbSe₂. On the basis of a sixfold perturbation, Gygi and Schlüter[17] explained that the lower and higher energy stars observed by STM were interpreted as bonding or antibonding states. The STM results (1) and (2) listed in Sec. 2.1 were able to be explained by this perturbation scheme. They adopted a sixfold crystal lattice potential in NbSe₂ as the perturbation. Recently, Zhu, Zhang, and Sigrist[61] investigated the effect of the underlying crystal lattice by means of a non-perturbation method, i.e., a method of diagonalizing a tight-binding Bogoliubov-de Gennes (BdG) Hamiltonian in a discrete square lattice, where the crystal lattice potential, i.e., the band structure is determined a priori. This method supplements the perturbation theory of Ref. [17]: the absolute orientation of the star relative to the underlying crystal lattice was determined[61].

By this non-perturbation approach, also a gradual rotation of the star-shaped LDOS was obtained in the intermediate energy region[61]. Nevertheless, it is not yet clear whether the crystal lattice effect is able to reproduce the remaining experimental findings (3) and (4), i.e., the split parallel ray structure and the behavior of peaks in the spectral evolutions. The model used in Ref. [61] is the discrete lattice model, and therefore it is impossible to obtain detailed spectra, e.g., spectral evolutions along radial lines, due to the discreteness. Hence, it is desired to treat the crystal lattice potential effect with a non-perturbation method in the continuum limit.

Now, the crystal lattice potential determines the band structure, and influences the structure of the Fermi surface. The effect of the crystal lattice potential should appear as the anisotropy of the Fermi surface. In our framework, the anisotropy of the Fermi surface is taken into account by assuming an anisotropic density of states at the Fermi surface, $\rho(\theta)$, which appears in the θ -integral of Eq. (2.10), and the anisotropic Fermi velocity $v_F(\theta)$, which appears in the Eilenberger (or Riccati) equations. The experimental findings (1)–(4) can be reproduced qualitatively, if we introduce a large anisotropy in $v_F(\theta)$.

Gygi and Schlüter considered also the effect of nearest-neighbor vortices, i.e, that of the vortex lattice[17]. They adopted a sixfold anisotropy of the vector potential as the vortex lattice effect, and treated it as the perturbation. However, the periodicity of the pair potential is also an important effect of the vortex lattice, as pointed out by Klein and Pöttinger[30, 33]. In extreme type-II superconductors such as NbSe₂ where $\kappa \gg 1$, the periodicity of the pair potential is expected to have stronger effects upon the structure of the LDOS than the anisotropy of the vector potential does. We find in Ref. [42] that the effect of the periodicity gives a characteristic sixfold structure to the LDOS.

This structure of the LDOS which results from the periodicity of the pair potential appears only at high magnetic fields such as 1 T for the material parameters appropriate to NbSe₂, where the vortex core regions substantially overlap each other[42]. At a lower magnetic field such as 0.1 T, the calculated

LDOS reduces to the almost circular structure. On the other hand, the LDOS observed in a STM experiment exhibits the star-shaped structure in spite of a low field 0.025 T (see Fig. 12 in Ref. [62]). Therefore, in the case of NbSe₂ at low magnetic fields, we need to consider the effects of anisotropy other than the vortex lattice effect in order to explain the star-shaped LDOS. Both the vortex lattice effect and the anisotropic superconducting gap one are important for the star-shaped LDOS observed in NbSe₂ at high magnetic fields. We expect a future STM experiment to be performed on isotropic superconducting compounds or metals to clarify the vortex lattice effect and confirm predictions of Ref. [42].

In STM experiments on NbSe₂, one of the directions of nearest-neighbor vortices coincides with the a axis (see the literature by Hess *et al.* [8, 6, 12, 13, 14, 15, 62, 63] or Renner *et al.*[25]), except for extreme low fields[64]. This experimental fact gives evidence of a correlation of the vortex lattice with the underlying crystal lattice of NbSe₂. It was recently found that in d -wave superconductors, higher-order (nonlocal correction) terms in the Ginzburg-Landau equation, which reflect the fourfold symmetric property of the d -wave pairing, give rise to a preferred direction of the vortex lattice[65, 66, 67]. In NbSe₂, the sixfold anisotropic pairing, Eq. (2.15), is expected to give rise to the same correlation as the d -wave pairing does, and it may be the origin of the experimental fact mentioned above. A possibility of the correlation of the vortex lattice with the underlying crystal lattice was recently reported also in a high- T_c cuprate[68, 69].

2.5.2 Beyond the quasiclassical approach

We mention the LDOS around a vortex in high- T_c cuprates. It seems from various experiments that high- T_c material is a d -wave superconductor[70]. A fourfold structure of the LDOS is predicted in d -wave superconductors by theoretical studies based on the quasiclassical theory[34, 35, 39]. The origin of this fourfold structure is same as that discussed in the present chapter for the gap anisotropy. Recently, Maggio-Aprile *et al.* observed tunneling spectra around vortices in a high- T_c cuprate, YBa₂Cu₃O_{7- δ} , with STM[18, 71, 69]. However, the spectroscopic images of STM have not exhibited any sign of a fourfold structure yet. We expect further detailed experiments to observe the fourfold symmetric LDOS structure.

When we consider the high- T_c materials, the quantum effects should be taken into account. The quasiclassical theory is certainly valid only in systems where the atomic scale spatial variation of the Green's function can be neglected with respect to the coherence length scale one[38, 72]. The effects neglected in the quasiclassical theory can be important in the case of the high- T_c cuprate; the quantization of energy levels of the bound states cannot be treated by the quasiclassical theory, and while it is possible in the quasiclassical approximation to divide the equation into individual equations for each direction of \vec{k} , it is impossible in the quantum-mechanical limit. Although we expect the fourfold structure of the LDOS should be observed in future experiments, the above effects may change the situation in the case of the high- T_c cuprate. It is certainly desired on the theoretical side that a fully quantum-mechanical approach clears up this problem in future.

As for the fully quantum-mechanical approach, it is needed to solve the BdG equation without quasiclassical approximations. The BdG equation cannot be

written in a local form in the case of an anisotropic pairing, and therefore it is difficult to treat this equation in the continuum limit. One of the possible approaches to this problem is the method of diagonalizing a BdG Hamiltonian for a specific lattice model[61, 73, 74, 75, 76]. In the lattice model, however, the atomic scale variation of wave functions among the lattice points is uncertain.

In most superconductors ($\xi \gg 1/k_F$), the atomic scale variation of the wave function is a redundant information and can usually be neglected on the basis of the quasiclassical theory. On the other hand, in the high- T_c cuprate superconductors, $k_F \xi \simeq \varepsilon_F/\Delta_0 \sim 1$ (the Fermi wave-number and energy are k_F and ε_F , respectively)[72], and therefore the atomic scale variation and the quantization of bound states in a vortex may be crucial for the electronic structure around the vortex in the cuprates.

The high- T_c cuprate is certainly the only superconductor possessed of a possibility of an experimentally detectable quantization in the vortex bound states. According to Ref. [3], a substantial energy quantization (of the order of $\Delta_0^2/\varepsilon_F \sim 10$ K) is expected to exist in the high- T_c cuprate. However, to the present author's knowledge, the system considered in Ref. [3] is an isotropic *s*-wave superconductor and the mechanism of the quantization in the case of anisotropic pairing is not yet understood. In case of gap node due to anisotropic pairing, it is expected that the separation of the energy levels becomes small. Further experiments, which, e.g., investigate spatial variation of this quantized bound states in the high- T_c cuprates with STM and then compare its result with the quasiclassical prediction[34, 35, 39] in order to clarify how the quantum effects mentioned above modify the vortex bound states, are the need for alternative theoretical studies of the vortex bound states.

2.5.3 Concluding remarks

The electronic structure of vortices in a compound, $\text{LuNi}_2\text{B}_2\text{C}$, was quite recently investigated by STM[77]. Although no conductance peaks related to localized quasiparticle states in the vortex core are observed in the experiment, due to a short mean free path (of the order of the coherence length) and thermal broadening effects at 4.2 K ($T_c \approx 16$ K)[77], a rich (maybe fourfold) structure of the LDOS such as that discussed in the present chapter is expected to be detected in STM spectra by lowering the temperature and decreasing impurities or defects. If an anisotropic bound states around a single vortex is observed, it should suggest an anisotropy of the pairing in this compound. The direction (in the k -space) in which the superconducting gap is suppressed corresponds to that (in the real space) of a ray of the LDOS at zero bias.

Finally, low-temperature STM is the unique experimental method which has the ability not only to image the distribution of the vortex lattice, but also to probe the electronic structure of individual vortices. We expect future STM experiments to be performed in vortex states on various superconductors such as organic conductors, high- T_c cuprates, heavy fermion superconductors (e.g., UPt_3), and a recently discovered non-copper-layered perovskite superconductor, Sr_2RuO_4 [78] which has nearly cylindrical Fermi surfaces[79, 80] and a possibility that an odd-parity superconductivity would be realized in it[81, 82]. The information on the vortex bound states available from STM spectra can be one of clues to the pairing. The low-temperature STM experiments deserve a great deal of attention.

Chapter 3

Quantum-Limit Property of a Vortex

3.1 Introduction

Growing interest has been focused on vortices both in conventional and unconventional superconductors from fundamental and applied physics points of view. This is particularly true for high- T_c cuprates, since it is essential that one understands fundamental physical properties of the vortices in the compounds to better control various superconducting characteristics of some technological importance. Owing to the experimental developments, it is not difficult to reach low temperatures of interest where distinctive quantum effects associated with the discretized energy levels of the vortex bound states are expected to emerge. The quantum limit is realized at the temperature where the thermal smearing is narrower than the discrete bound state levels[22]: $T/T_c \leq 1/(k_F \xi_0)$ with $\xi_0 = v_F/\Delta_0$ the coherence length (Δ_0 the gap at $T = 0$) and k_F (v_F) the Fermi wave number (velocity). For example, in a typical layered type-II superconductor NbSe₂ with $T_c = 7.2$ K and $k_F \xi_0 \sim 70$, the quantum limit is reached below $T < 100$ mK. As for the high- T_c cuprates, the corresponding temperature is rather high: $T < 10$ K for YBa₂Cu₃O_{7- δ} (YBCO).

Important microscopic works to theoretically investigate the quasiparticle spectral structure around a vortex in a clean limit are put forth by Caroli *et al.*[3, 83], Kramer and Pesch[22], and Gygi and Schlüter[16]. The low-lying excitations are essential to correctly describe low- T thermodynamic and transport properties in the vortex state (or the mixed state). These include anomalous electric[84, 85] or thermal Hall conductivity[86] and mysterious observations of the quantum magnetic dHvA oscillations[87]; various topics are debated intensively[88]. Yet there has been no serious attempt or quantitative calculation to explore deep into the quantum regime.

The purposes of the present chapter are to reveal the quantum-limit aspects of the single vortex in s -wave superconductors and to discuss a possibility for the observation of them.

The present study is motivated by the following recent experimental and theoretical situations: (1) The so-called Kramer-Pesch (KP) effect[22, 16, 89, 90]; a shrinkage of the core radius upon lowering T (to be exact, an anomalous

increase in the slope of the pair potential at the vortex center at low T) is now supported by some experiments[91]. The T dependence of the core size is studied by μ SR on NbSe₂[92] and YBCO[93], which is discussed later. The KP effect, if confirmed, forces us radically alter the traditional picture[1] for the vortex line such as a rigid normal cylindrical rod with the radius ξ_0 . (2) The scanning tunneling microscopy (STM) experiment on YBCO by Maggio-Aprile *et al.*[18], which enables us to directly see the spatial structure of the low-lying quasiparticle excitations around the vortex, arouses much interest. They claim that surprisingly enough, there exist only a few discretized bound-state levels in the vortex core, i.e., the vortex is almost “empty.” It resembles our naive image for conventional s -wave superconductors where in the quantum limit a few quantized levels of the bound states remain inside the bulk energy gap Δ_0 . (3) The theoretical situation on this subject[18] is still very confusing; Some[74, 94] claim that the bound-state energy levels are not discretized for d -wave pair, but discretized for s -wave pair. Some[72] claim the discretized-like structure even for the former. For s -wave case, where the formulation of the problem is well defined, we should establish our understanding of the vortex structure in the quantum limit. (4) Lastly, we are motivated by a curiosity; Previously we have calculated the local density of states (LDOS) for s -wave pair on the basis of the quasiclassical (Eilenberger) theory[41, 95, 42], successfully applied to the STM observations on NbSe₂ done by Hess *et al.*[8, 6, 12, 13, 14, 15]. We are particularly interested in what happens in LDOS at further lower T , say, below 50 mK deep into the quantum limit, at which it may be now feasible to perform STM experiments.

Prompted by these motivations, we self-consistently solve the Bogoliubov-de Gennes (BdG) equation[4], which is one of the most fundamental microscopic equations of superconductivity and contains fully quantum effects.

3.2 Bogoliubov-de Gennes theory

We start with the BdG equations for the quasiparticle wave functions $u_j(\mathbf{r})$ and $v_j(\mathbf{r})$ labeled by the quantum number j :

$$\begin{aligned} \left[\frac{-1}{2k_F\xi_0} \nabla^2 - E_F \right] u_j(\mathbf{r}) + \Delta(\mathbf{r})v_j(\mathbf{r}) &= E_j u_j(\mathbf{r}), \\ - \left[\frac{-1}{2k_F\xi_0} \nabla^2 - E_F \right] v_j(\mathbf{r}) + \Delta^*(\mathbf{r})u_j(\mathbf{r}) &= E_j v_j(\mathbf{r}), \end{aligned} \quad (3.1)$$

in a dimensionless form, where $\Delta(\mathbf{r})$ is the pair potential and $E_F (=k_F\xi_0/2)$ the Fermi energy. The length (energy) scale is measured by ξ_0 (Δ_0). For an isolated single vortex in an extreme type-II superconductor, we may neglect the vector potential in Eq. (3.1). The pair potential is determined self-consistently by

$$\Delta(\mathbf{r}) = g \sum_{|E_j| \leq \omega_D} u_j(\mathbf{r})v_j^*(\mathbf{r}) \{1 - 2f(E_j)\} \quad (3.2)$$

with the Fermi function $f(E)$. Here, g is the coupling constant and ω_D the energy cutoff, which are related by the BCS relation via the transition temperature T_c and the gap Δ_0 . We set $\omega_D = 10\Delta_0$. The current density is

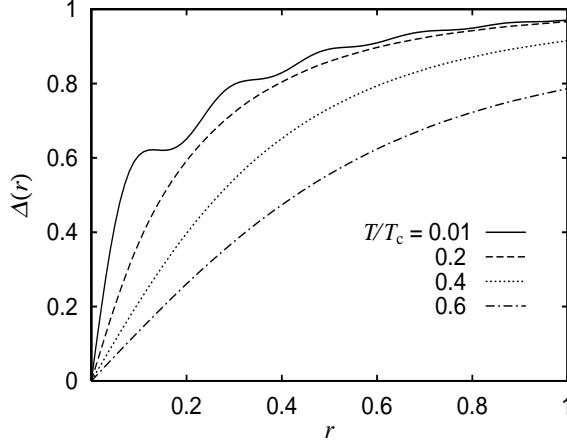


Figure 3.1: The spatial variation of the pair potential $\Delta(r)$ normalized by Δ_0 around the vortex for several temperatures and $k_F\xi_0 = 16$. The length r is measured by ξ_0 .

given by $\mathbf{j}(\mathbf{r}) \propto \text{Im} \sum_j [f(E_j)u_j^*(\mathbf{r})\nabla u_j(\mathbf{r}) + \{1 - f(E_j)\}v_j(\mathbf{r})\nabla v_j^*(\mathbf{r})]$. We consider an isolated vortex under the following conditions. (a) The system is a cylinder with a radius R . (b) The Fermi surface is cylindrical, appropriate for the materials such as NbSe₂ and high- T_c cuprates. (c) The pairing has isotropic s -wave symmetry. Thus the system has a cylindrical symmetry. We write the eigenfunctions as $u_j(\mathbf{r}) = u_{n\mu}(r) \exp[i(\mu - \frac{1}{2})\theta]$ and $v_j(\mathbf{r}) = v_{n\mu}(r) \exp[i(\mu + \frac{1}{2})\theta]$ with $\Delta(\mathbf{r}) = \Delta(r) \exp[-i\theta]$ in polar coordinates, where n is a radial quantum number and the angular momentum $|\mu| = \frac{1}{2}, \frac{3}{2}, \frac{5}{2}, \dots$. We expand the eigenfunctions in terms of the Bessel functions $J_m(r)$ as $u_{n\mu}(r) = \sum_i c_{ni} \phi_{i|\mu - \frac{1}{2}|}(r)$ and $v_{n\mu}(r) = \sum_i d_{ni} \phi_{i|\mu + \frac{1}{2}|}(r)$ with $\phi_{im}(r) = \frac{\sqrt{2}}{R J_{m+1}(\alpha_{im})} J_m(\alpha_{im} r/R)$, ($i = 1, 2, \dots, N$, and α_{im} is the i -th zero of $J_m(r)$). The BdG is reduced to a $2N \times 2N$ matrix eigenvalue problem[16]. Our system is characterized by $k_F\xi_0$, which is a key parameter of the present problem.

3.3 Results

In Fig. 3.1, the calculated spatial variation of $\Delta(r)$ is displayed for various T . It is seen that as T decreases, the core size ξ_1 defined by $\xi_1^{-1} = \lim_{r \rightarrow 0} \Delta(r)/(r\Delta_\infty(T))$ shrinks and the oscillatory spatial variation with a wave length $\sim 1/k_F$ becomes evident in $\Delta(r)$ [22, 16]. The physical reason for this Friedel-like oscillation lies in the following facts. All eigenfunctions $u_{n\mu}(r)$ and $v_{n\mu}(r)$ contain a rapid oscillation component with $1/k_F$. At lower T the lowest bound states, whose oscillation amplitude is large near the core, dominate physical quantities. We note that the oscillatory behavior can always appear at sufficiently low T irrespective of values of $k_F\xi_0$. We also mention that a similar oscillatory spatial variation around a vortex core in the Bose condensate of ⁴He is found theoretically, due to the roton excitations[96].

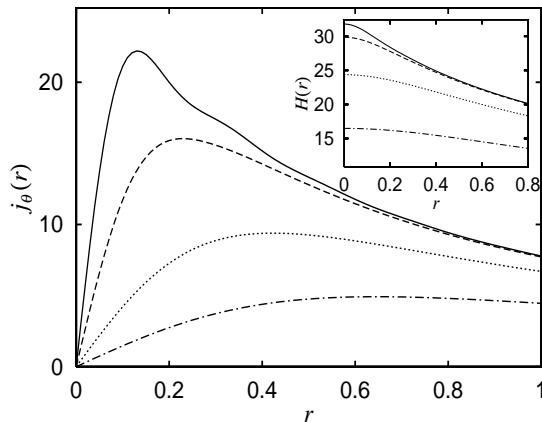


Figure 3.2: The current distribution normalized by $c\phi_0/(8\pi^2\xi_0^3\kappa^2)$ for several temperatures, where ϕ_0 is the flux quantum and $\kappa (\gg 1)$ is the GL parameter. The inset shows the field distribution normalized by $\phi_0/(2\pi\xi_0^2\kappa^2)$. The temperatures are the same as in Fig. 1, and $k_F\xi_0 = 16$.

The associated supercurrent $j_\theta(r)$ and the field $H(r)$ are shown in Fig. 3.2. Reflecting the above oscillation, $j_\theta(r)$ also exhibits a weak oscillation around $r = 0.2-0.5 \xi_0$. It is difficult to see the oscillation in $H(r)$, because it is obtained by integrating $j_\theta(r)$ via the Maxwell equation $\nabla \times \mathbf{H} = \frac{4\pi}{c} \mathbf{j}(r)$, resulting in a smeared profile. It is also seen that the position of the maximum of $j_\theta(r)$ becomes shorter as T decreases. These features quite differ from those obtained within the Ginzburg-Landau (GL) framework[1, 97].

The T dependence of $\xi_1(T)$ for various $k_F\xi_0$ values is shown in Fig. 3.3. Coinciding with Kramer and Pesch[22] for s -wave pair and Ichioka *et al.*[90] for d -wave pair, $\xi_1(T)$ decreases almost linearly with T , that is, $\xi_1(T)/\xi_0 \sim T/T_c$ except at extremely low T . An important difference from these quasiclassical theories[22, 90] appears at lower T . At a lower $T < T_0 \simeq T_c/(k_F\xi_0)$, where the quantum limit is realized, the shrinkage of the core size stops to saturate, and the saturated value is estimated as $\xi_1/\xi_0 \sim (k_F\xi_0)^{-1}$.

According to the μ SR experimental data[92, 93], the core radius in NbSe₂ shows a strong T dependence, while that in YBCO with $T_c=60$ K is almost T -independent below $\sim 0.6T_c$. This seemingly contradicting result can be understood as follows. The strong T dependence in NbSe₂ is the usual KP effect corresponding to the curves for larger $k_F\xi_0$ in Fig. 3.3. At lower T than T_0 estimated as ~ 100 mK ($k_F\xi_0 \sim 70$), the shrinkage must saturate (the above experiment is done above ~ 2 K). As for the YBCO data, since the estimated $k_F\xi_0$ is small (~ 4 [18] for YBCO with $T_c=90$ K), the saturation is already attained at a relatively high T such as shown in Fig. 3.3. Thus the absence or weakness of the KP effect in YBCO is simply attributable to the fact that the quantum-limit temperature T_0 is quite high.

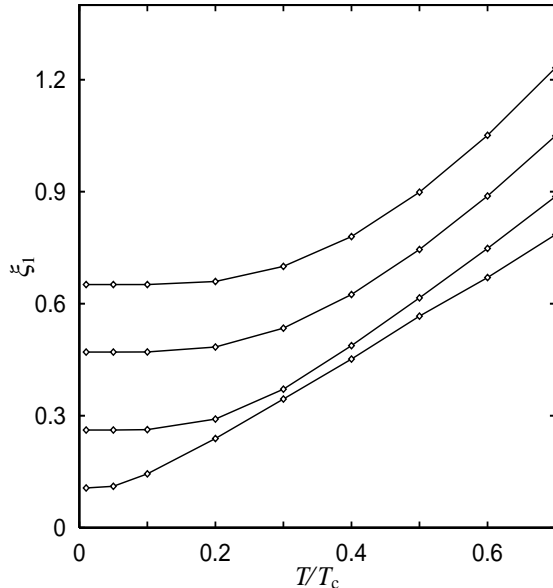


Figure 3.3: The T dependence of the vortex radius ξ_1 normalized by ξ_0 for several $k_F\xi_0$ ($= 1.2, 2, 4,$ and 16 from top to bottom).

Reflecting the shrinkage of the core radius, the bound-state energies E_μ increases as T decreases. This T -dependent E_μ shift, due to the KP effect, and its saturation at lower T may lead to a nontrivial T dependence in thermodynamic and transport properties.

In Fig. 3.4, we plot the energy levels E_μ of the low-lying bound states ($\mu = \frac{1}{2}, \frac{3}{2}, \dots, \frac{13}{2}$) as a function of $k_F\xi_0$, at sufficiently low T ($T/T_c = 0.01$) where increasing of the energy levels saturates. It is seen that in large- $k_F\xi_0$ region, the bound states densely pack inside the gap Δ_0 , allowing us to regard them as continuous ones. This is the case where the quasiclassical approximation[22, 90] validates. In small- $k_F\xi_0$ region, where the quantum effect is important even at high T , only a few bound states remain within the low-energy region. We find that even for small $|\mu|$, the spacing between the energy levels E_μ is not constant, but rather becomes narrower as $|\mu|$ increases. The often adopted formula $E_\mu/\Delta_0 = 2\mu/(k_F\xi_0) \propto 2\mu/(k_F\xi_1)$ due to Caroli *et al.*[3, 83], or $E_\mu/\Delta_0 = (2\mu/k_F\xi_0) \ln[\xi_0/2\xi_1]$ by Kramer and Pesch in the limit $\xi_1 \ll \xi_0$ [22] do not satisfactorily explain our self-consistent results. Instead, our result is empirically fitted to a formula $E_{1/2}/\Delta_0 = (0.5/k_F\xi_0) \ln[k_F\xi_0/0.3]$ for large $k_F\xi_0$ as shown in the dotted curve in Fig. 3.4.

In Fig. 3.5, the spectral evolution, i.e., the spatial variation of LDOS, which is calculated by $N(\mathbf{r}, E) \propto \sum_j [|u_j(\mathbf{r})|^2 f'(E - E_j) + |v_j(\mathbf{r})|^2 f'(E + E_j)]$, is shown for $k_F\xi_0=8$ at low temperature $T=0.05T_c$. It is well contrasted with that of the higher T case by Gygi and Schlüter[16] (see, for comparison, Fig. 15 in Ref. [16] where $k_F\xi_0 \sim 70$ and $T \simeq 0.13T_c$, calculated under the two-dimensional Fermi surface). As lowering T , because of the quantum effects, the thermally smeared spectral structure drastically changes and becomes far finer

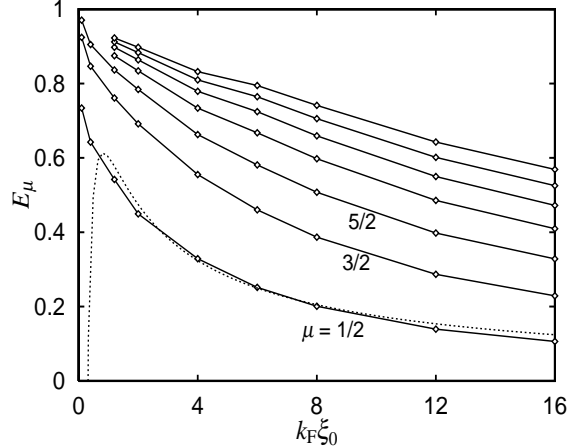


Figure 3.4: The lowest seven bound-state energies E_μ , normalized by Δ_0 , as a function of $k_F \xi_0$, at enough low temperature $T/T_c = 0.01$. The dotted line is a fitting curve (see the text).

one around the vortex. The spectra are discretized inside the gap and consist of several isolated peaks, each of which precisely corresponds to the bound states E_μ ($|\mu| = \frac{1}{2}, \frac{3}{2}, \dots$). Reflecting the oscillatory nature of the eigenfunctions $u_\mu(r)$ and $v_\mu(r)$ with the period $1/k_F$, the spectral evolution also exhibits the Friedel-like oscillation as seen from Fig. 3.5.

To show clearly the particle-hole asymmetry of the LDOS of Fig. 3.5, which is another salient feature, we present in Fig. 3.6 the spectra at the vortex center $r = 0$ and $0.2\xi_0$ [We can barely see the asymmetry in Wang and MacDonald[74] (see Fig. 3(a) in Ref. [74])]. At the center $r = 0$, the bound-state peak with $E_{1/2}$, which comes from $u_{1/2}$ and $v_{-1/2}$, appears on $E > 0$ side and other peaks for $|E_\mu| < \Delta_0$ (which include $E_{-1/2}$) vanish at $r = 0$, because only $u_{1/2}(r)$ and $v_{-1/2}(r) \propto J_0(r = 0) \neq 0$. The particle-hole asymmetry in the vortex bound states appears even if the normal-state density of states is symmetric. These features are subtle[16] or absent[95] in the previous calculations. This asymmetry around the vortex is quite distinctive, should be checked by STM experiments, and may be crucial for the Hall conductivity in the mixed state.

Let us argue some of the available experimental data in the light of the present study. The lowest bound state level $E_{1/2}/\Delta_0$ is estimated by Maggio-Aprile *et al.*[18] for YBCO with $T_c=90$ K ($E_{1/2}=5.5$ meV and $\Delta_0=20$ meV), yielding $k_F \xi_0 \sim 4$. Since it implies that ξ_0 is only of the order of the crystal-lattice constant, we should caution that Maggio-Aprile *et al.*[18] take their data for the spectral evolution every 10 \AA apart near the core, thus the important spatial information on LDOS might be lost. So far the existing STM data[18, 15, 77] taken at the vortex center are almost symmetric about $E=0$, e.g., on NbSe₂ at $T=50$ mK[15]. The reason why the so-called zero-bias peak is centered just symmetrically at $E=0$ is that $k_F \xi_0$ is large and T is too high to observe the quantum effects.

We emphasize that in any clean s -wave type-II superconductors at appropriately low T ($< T_0 \simeq T_c/(k_F \xi_0)$), one can observe these eminent characteristics

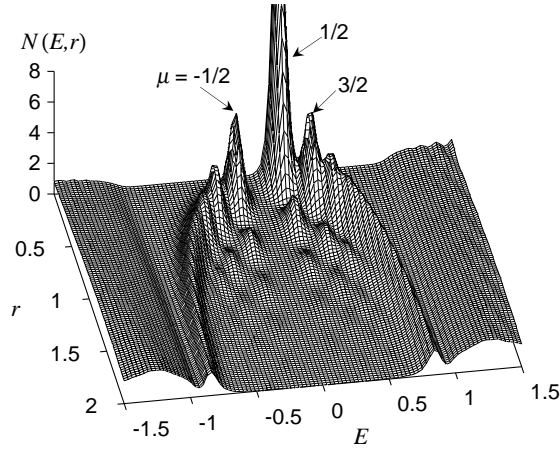


Figure 3.5: The spectral evolution $N(E, r)$ at $T/T_c = 0.05$ and $k_F \xi_0 = 8$. It is normalized by the normal-state density of states at the Fermi surface. E and r are measured by Δ_0 and ξ_0 , respectively.

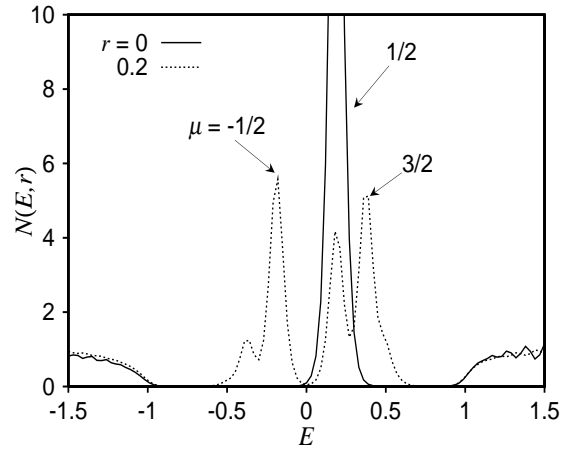


Figure 3.6: The local density of states $N(E, r)$ at $r = 0$ (solid line) and $0.2\xi_0$ (dotted line). $T/T_c = 0.05$ and $k_F \xi_0 = 8$.

associated with the quantum effects. We should note also that a vortex in superfluid neutron star matters is a candidate for the extreme quantum-limit vortex[98].

3.4 Summary

We have analyzed the vortex core structure and the related quasiparticle energy spectrum by self-consistently solving the BdG equation for an isolated vortex in a clean s -wave type-II superconductor, focusing on the low- T quantum effects. We have found the far richer structure in the pair potential, supercurrent, and LDOS than what one naively imagines from the corresponding calculations done at high T or $k_F \xi_0 \gg 1$ [16, 95], and pointed out experimental feasibility to observe it.

The widely used working hypothesis for the vortex core of a rigid normal rod with the radius ξ_0 [1] must be cautiously used for the clean superconductors of interest: the magnetic field distribution probed by neutron diffraction[99, 100] or μ SR[92, 93, 101] through the magnetic form factor analysis based on the GL theory[102] must be taken with caution. Detailed investigations of various mysteries associated with the vortices, e.g., the Hall effect in the mixed state[84, 85] and the thermal Hall conductance[86] belong to future work.

Chapter 4

Electric Charging of a Vortex Core

4.1 Introduction

Electric charging phenomena around vortices have the potential of becoming one of the key features in the physics of the mixed state in type-II superconductors. Until quite recently, little was known about the electric charging inherent in vortices, while it has been well recognized since the 1950's that each vortex line carries a quantized magnetic flux. Only recently, it was noticed that an electric charge accumulates around a static vortex line in type-II superconductors. Khomskii and Freimuth[103], and Blatter *et al.*[104] theoretically discussed the electric charging around a vortex[105]. If the electric charging of vortices is experimentally confirmed, it will open the door to an unexplored field in which one expects various electromagnetic phenomena to originate from the electric charge trapped by vortices.

In spite of the growing interest in vortex core charging, firm experimental evidence of the charging is lacking at present. However, various experimental attempts are now in progress and are on the verge of detecting a charge accumulation inside vortex cores. One such experiment is a spin-polarized neutron scattering investigation of the flux line lattice in Nb by Neumann *et al.*[106] They detected a nonzero nuclear contribution to the Bragg peaks corresponding to the periodicity of the flux line lattice. This experimental result strongly suggests existence of the vortex core charge; if each vortex constituting the flux line lattice traps electrons or holes, the response of the underlying nuclei to these will induce a distortion of the nuclear lattice around the vortices[106, 107]. Various types of experiments which will attempt to detect the vortex core charge are also planned. In addition, an experiment to observe the temperature T and magnetic field H dependence of the vortex core charge is expected in order to establish the existence of the vortex core charging. Therefore, it is certainly desired that detailed theoretical predictions for the temperature or magnetic field dependence of the vortex core charge should be presented for experimental verification.

In this chapter, we present the structure of the carrier density around a static single vortex and its temperature dependence, solving self-consistently

the Bogoliubov-de Gennes (BdG) equation[4]. On the basis of the solutions of the BdG equation, we discuss not only the temperature dependence but also the relation between the charging of the vortex core and the so-called Caroli-de Gennes-Matricon (CdGM) states (or the vortex bound states).

The CdGM states, i.e., low-energy excited states due to vortices, were first discussed theoretically by Caroli *et al.*[3] Their existence was experimentally confirmed by Hess *et al.*[6, 12], who observed spatial dependence of the excitation spectra around a vortex with scanning tunneling microscopy (STM). The local density of states (LDOS) around a vortex, probed by STM, depends on the Bogoliubov wave functions of the CdGM states $u_j(\mathbf{r})$ and $v_j(\mathbf{r})$, labeled by the quantum number j . The LDOS $N(\mathbf{r}, E)$ (to be exact, thermally smeared LDOS, i.e., the tunneling conductance) is given as

$$N(\mathbf{r}, E) = - \sum_j [|u_j(\mathbf{r})|^2 f'(E - E_j) + |v_j(\mathbf{r})|^2 f'(E + E_j)], \quad (4.1)$$

where E_j is the eigenenergy and $f(E)$ the Fermi function (the prime represents the derivative). The STM enable us to extract detailed information on the wave functions around a vortex. Here, we notice that the carrier density around a vortex, $n(\mathbf{r})$, also relates to these wave functions:

$$n(\mathbf{r}) = 2 \sum_{E_j > 0} [|u_j(\mathbf{r})|^2 f(E_j) + |v_j(\mathbf{r})|^2 \{1 - f(E_j)\}]. \quad (4.2)$$

The electric charging (or the inhomogeneous electron density distribution) around a vortex is related to the LDOS through the wave functions $u_j(\mathbf{r})$ and $v_j(\mathbf{r})$. This suggests unique potential ability of the STM; the structure of the LDOS probed by STM relates to the spatial structure of the vortex core charge.

Regarding the previous theories of the mechanism of the vortex core charging, Khomskii and Freimuth[103] based their scenario on a normal-core model. Assuming that the vortex core is a region of normal metal surrounded by a superconducting material, they considered that the corresponding difference in the chemical potential[108] leads to a redistribution of the electrons[103]. Blatter *et al.*[104] discussed the charging mechanism, considering spatial variation of the pair potential $\Delta(\mathbf{r})$ around a vortex. On the basis of the zero-temperature version of Eq. (4.2), they obtained $n(\mathbf{r})$ by combining the spatial variation of the wave function $v(\mathbf{r})$ with particle-hole asymmetry in the normal-state density of states at the Fermi level. The discussion was, however, based on a wave function which was the same form as the *uniform solution* of the BdG equation, namely[104]

$$v_k(\mathbf{r}) = \sqrt{\frac{1}{2} \left(1 - \frac{\xi_k}{E_k}\right)}, \quad E_k = \sqrt{\xi_k^2 + |\Delta(\mathbf{r})|^2}. \quad (4.3)$$

The spatial variation of $v_k(\mathbf{r})$ was directly determined by the local value of $\Delta(\mathbf{r})$, which is not exactly appropriate for the vortex system. It is desired that one should base the calculation on the exact wave functions of the CdGM states.

Prompted by this motivation, we will self-consistently solve the BdG equation to obtain the exact wave functions $u_j(\mathbf{r})$ and $v_j(\mathbf{r})$ of the CdGM states (including the extended states above the gap).

4.2 Formulation

We start with the BdG equation[4] given, in a dimensionless form, by

$$\begin{aligned} \left[\frac{-1}{2k_F\xi_0} \nabla^2 - \mu \right] u_j(\mathbf{r}) + \Delta(\mathbf{r})v_j(\mathbf{r}) &= E_j u_j(\mathbf{r}), \\ - \left[\frac{-1}{2k_F\xi_0} \nabla^2 - \mu \right] v_j(\mathbf{r}) + \Delta^*(\mathbf{r})u_j(\mathbf{r}) &= E_j v_j(\mathbf{r}), \end{aligned} \quad (4.4)$$

where μ is the chemical potential and $\xi_0(=v_F/\Delta_0)$ is the coherence length [Δ_0 is the uniform gap at $T = 0$, and k_F (v_F) is the Fermi wave number (velocity)]. In Eq. (4.4), the length (energy) scale is measured by ξ_0 (Δ_0). For an isolated single vortex in an extreme type-II superconductor, we may neglect the vector potential in Eq. (4.4). To maintain macroscopic charge neutrality in the material, in Eq. (4.2) we constrain the electron density in a uniform system to be constant on the temperatures. We use μ determined at each temperature by this constraint, which is equivalent at zero temperature to Eq. (4) of Ref. [108]. The pair potential is determined self-consistently by

$$\Delta(\mathbf{r}) = g \sum_{|E_j| \leq \omega_D} u_j(\mathbf{r})v_j^*(\mathbf{r})\{1 - 2f(E_j)\}, \quad (4.5)$$

where g is the coupling constant and ω_D the energy cutoff, which are related by the BCS relation via the transition temperature T_c and the gap Δ_0 . We set $\omega_D = 20\Delta_0$. We consider, for clarity, an isolated vortex under the following conditions. (a) The system is a cylinder with a radius R . (b) The Fermi surface is cylindrical. (c) The pairing has isotropic s -wave symmetry. Thus the system has cylindrical symmetry. We write the eigenfunctions as $u_j(\mathbf{r}) = u_{n,l}(r) \exp[i(l - \frac{1}{2})\theta]$ and $v_j(\mathbf{r}) = v_{n,l}(r) \exp[i(l + \frac{1}{2})\theta]$ with $\Delta(\mathbf{r}) = \Delta(r) \exp[-i\theta]$ in polar coordinates, where n is the radial quantum number and the angular momentum $|l| = \frac{1}{2}, \frac{3}{2}, \frac{5}{2}, \dots$. We expand the eigenfunctions in terms of the Bessel functions[3] $J_m(r)$ as[16]

$$\begin{aligned} u_{n,l}(r) &= \sum_{i=1}^N c_{ni} \phi_{i|l-\frac{1}{2}|}(r), \\ v_{n,l}(r) &= \sum_{i=1}^N d_{ni} \phi_{i|l+\frac{1}{2}|}(r), \end{aligned} \quad (4.6)$$

where $\phi_{im}(r) = [\sqrt{2}/R J_{m+1}(\alpha_{im})] J_m(\alpha_{im}r/R)$ and α_{im} is the i -th zero of $J_m(r)$. We set $R = 20\xi_0$. The BdG equation is reduced to a $2N \times 2N$ matrix eigenvalue problem. This useful technique to solve Eq. (4.4), developed by Gygi and Schlüter[16], has been utilized in some cases[16, 109, 94, 110, 111, 112, 98, 9]. Our system is characterized by a parameter $k_F\xi_0$ [111, 112, 9], important for the present problem. From our standpoint, all interactions between the quasiparticles are renormalized to g in Eq. (4.5) and additional screening does not exist in the Hamiltonian. The screening for the charge ordering is excluded as in the charge density wave studies[113]. If some screening effect is considered, in

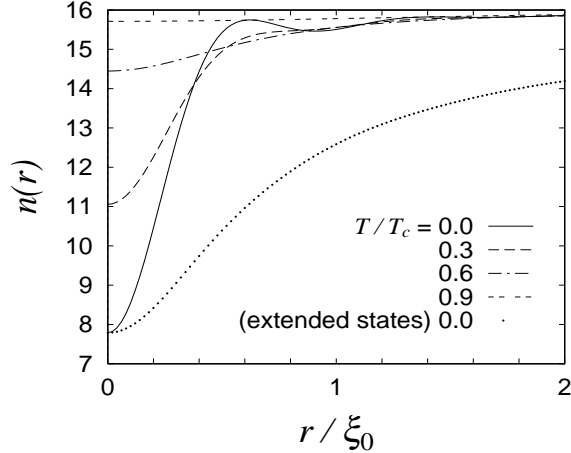


Figure 4.1: The spatial variation of the carrier density $n(r)$ (in arbitrary units) around the vortex for several temperatures and $k_F \xi_0 = 4$. The contribution of the extended states to $n(r)$ at $T = 0$ is shown by the dotted line. The difference between this contribution and the total $n(r)$ at $T = 0$ is the contribution of the bound states.

principle we may take it into account as an external potential in Eq. (4.4) and solve self-consistently the equations together with an additional equation, e.g., the Poisson's equation. Such a study, if meaningful, is left for a future work. Using the calculated $u_j(\mathbf{r})$ and $v_j(\mathbf{r})$, we obtain the LDOS $N(\mathbf{r}, E)$ and the carrier density $n(\mathbf{r})$ from Eqs. (4.1) and (4.2), respectively.

4.3 Results

In Fig. 4.1, we present the spatial structure of the carrier density $n(r)$ around the vortex at several temperatures. The Friedel oscillation appears at low temperatures, because each wave function of the low-energy CdGM states oscillates with a period $\simeq k_F^{-1}$. It is striking that the carrier density at the vortex center exhibits strong temperature dependence and leads to a substantial charging at low temperatures.

The carrier density at the vortex center in Fig. 4.1 decreases with respect to that far from the core. Consequently, in the case of the present electron system (i.e., the two-dimensional free electron system), the sign of the vortex core charge is opposite to the sign of the electron which is the dominant charge carrier in the present case. When the dominant charge carriers are holes, we only have to treat these holes as carriers in that system instead of the electrons and there are no changes in the formulation [Eqs. (4.1), (4.2), and (4.4)–(4.6)]. The density of the dominant carriers (holes) decreases near the vortex center in this case as well.

The density of the dominant carriers decreases near the vortex center, as long as the wave functions around a vortex for the dominant carriers are given by Eq. (4.6)[114]. This is related to particle-hole asymmetry in the LDOS

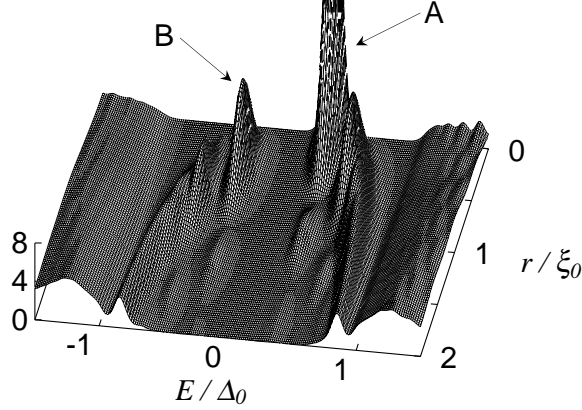


Figure 4.2: The spectral evolution of the LDOS $N(E, r)$ (in arbitrary units) at $T/T_c = 0.05$ and $k_F \xi_0 = 4$.

inside the vortex core and can be understood in connection with the CdGM states as follows. In the definition of the angular momentum l in Eq. (4.6), the bound-state energy spectrum is $E_l > 0$ for $l > 0$ (and $E_l < 0$ for $l < 0$), where $E_l = -E_{-l}$. In Fig. 4.2, we show the spectral evolution obtained from Eq. (4.1). In systems where $k_F \xi_0$ is small (the quantum limit), the asymmetry in the LDOS appears conspicuously. The two largest peaks near $E = 0$ are noticeable [the peaks A and B]. The peak A at $E = E_{l=1/2}$ (> 0) is composed of $|u_{l=1/2}(r)|^2 (= |v_{l=-1/2}(r)|^2)$. The peak B at $E = E_{-1/2}$ (< 0) is composed of $|v_{1/2}(r)|^2 (= |u_{-1/2}(r)|^2)$. From Eq. (4.6), $u_{1/2}(0) \neq 0$ and $v_{1/2}(0) = 0$ because $J_m(0) \neq 0$ only for $m = 0$. The asymmetry between $u_{1/2}(r)$ and $v_{1/2}(r)$ leads to the particle-hole asymmetry in the LDOS inside the core[9]. Now, according to Eq. (4.2), $n(r)$ is constructed from the wave functions which belong to $E > 0$. The contribution from the extended states ($E > \Delta_0$) is presented as the dotted line in Fig. 4.1. The remaining contribution to $n(r)$ come from the bound states. The lowest bound state $v_{1/2}(r)$, which belongs to the lowest bound state eigenenergy $E_{1/2} > 0$, predominantly determines the structure of $n(r)$ in the vicinity of the vortex center. The amplitude $|v_{1/2}(r)|^2$ is equal to that of the peak B in the LDOS. The spatial profile of $n(r)$ is determined by the shape of $|v_{1/2}(r)|^2$, i.e., the peak B. Since $|v_{1/2}(r)|^2$ decreases to zero with $r \rightarrow 0$ as seen from the spatial profile of the peak B in Fig. 4.2, we can infer that $n(r)$ decreases near the vortex center.

According to discussions[104] based on Eq. (4.3), the carrier density near the vortex center has a sensitive dependence on the slope in the density of states. It might be expected that if the derivative of the density of states is negative, the carrier density increases at the vortex center. To examine it, we have investigated the case of the energy band, $k^2/2m + k^4/4m^2\varepsilon_0$, (see Ref. [115]) which has a negative derivative of the density of states in two dimensions.

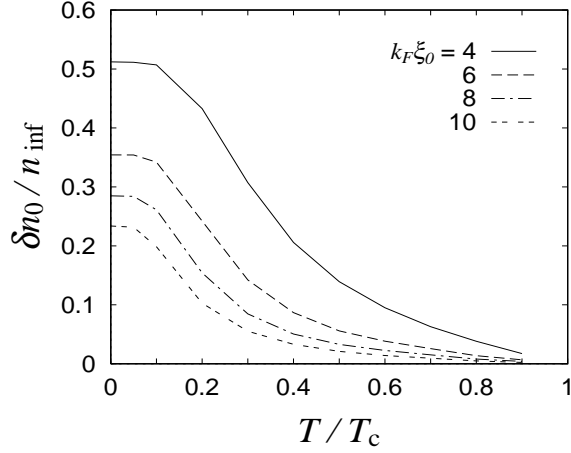


Figure 4.3: The temperature dependence of the carrier density $n_0 = n(r = 0)$ at the vortex center. In the figure $\delta n_0/n_\infty$ are plotted for several $k_F \xi_0$, where $\delta n_0 = |n_0 - n_\infty|$ and $n_\infty (\equiv n_{\text{inf}})$ is the plateau density far from the core.

In the calculation with a fixed μ , the carrier density far from the core certainly decreases with the growth of the gap $\Delta(T)$ on lowering T , which is consistent with the precondition of Ref. [104]. In this situation, on the basis of Eq. (4.3), the carrier density $n(r)$ is naively expected to recover to the normal-state value on approaching the center $r = 0$ where $\Delta(r) = 0$. $n(r)$ is then expected to increase at the center. However, according to results of the calculation based on the wave functions of the CdGM states, $n(r)$ decreases at the vortex center. We conclude that, the carrier density near the vortex center is determined by the electronic structure inside the vortex core, which is insensitive to the slope in the normal-state density of states at the Fermi level.

Let us focus on the magnitude of the core charge. The carrier density at the vortex center, from which the order of magnitude of the core charge is estimated, exhibits substantial temperature dependence as shown in Fig. 4.3. We plot $\delta n_0/n_\infty$, where $\delta n_0 = |n_0 - n_\infty|$, $n_0 = n(r = 0)$, and n_∞ is the plateau density $n_\infty = n(R/2)$, to which the calculated $n(r)$ settles away from the core. We note that the $k_F \xi_0$ dependence of the density, $\delta n_0/n_\infty \sim (k_F \xi_0)^{-\alpha} \simeq (\Delta_0/\varepsilon_F)^\alpha$, varies with the temperature (ε_F is the Fermi energy). Our numerical data show that $\alpha \approx 1$ near $T = 0$ and $\alpha \approx 2$ near $T = 0.5T_c$. The exponent α is crucial to the magnitude of the core charge. In most conventional superconductors, the parameter $k_F \xi_0$ is of the order of 100. It can be 1 – 10 in high- T_c cuprates. Depending on the estimate of α , there can appear substantial differences in the evaluation of the magnitude of the core charge. According to our results, α depends on the temperature as above. To estimate the total core charge Q_v per unit length along the vortex axis, we consider the charging volume in Fig. 4.1 to be a cone with a height δn_0 and a base radius r_1 ($2k_F r_1 = \pi$). $n(r)$ almost recovers to n_∞ initially at $r_1 \sim k_F^{-1}$ at low temperatures. Q_v is evaluated as $Q_v \approx e\pi r_1^2 \delta n_0/3$. We consider a pancake vortex in a layer, and the distance between each layer is d . In this case $n_\infty = 2\pi k_F^2 (2\pi/d)/8\pi^3$. We then obtain $Q_v \sim e(k_F \xi_0)^{-\alpha} d^{-1}$ at low temperatures.

4.4 Discussions

We should comment on the vortex dynamics in the context of the above temperature dependence of n_0 , although the issue concerning the dynamics is seriously controversial at the present time[116]. Feigel'man *et al.*[117] proposed a nondissipative transverse force acting on a vortex originating from δn_0 (see also Ref. [115]). Kopnin *et al.* reported that the effect proposed by Feigel'man *et al.*[117] can be understood from the viewpoint of the spectral flow theory, where n_0 is regarded as the spectral flow parameter C_0 [118, 119]. The parameter C_0 is independent of the temperature. Hence it appears to be inconsistent with the temperature dependence of n_0 presented in this chapter. Even in a neutral system with a fixed μ , n_0 exhibits substantial temperature dependence in our calculations. While Kopnin[120] discussed the temperature dependence of that force, the temperature dependence of δn_0 itself at the vortex center seems not to be explicitly included there. We hope for a further investigation based on the CdGM solutions[3] to reveal possible mutual relations between these theories (Refs. [117], [118], [119], and [120]) and the significant temperature dependence of $n(r)$ in the present paper[121].

We point out a relation between the present work and STM experiments. Maggio-Aprile *et al.*[18] and Renner *et al.*[19] observed spectral evolutions of the LDOS inside the vortex cores in the high- T_c cuprates. They detected particle-hole asymmetry in the LDOS near the core center (see Fig. 2 in Ref. [19]). We expect that the asymmetry observed in the experiments has the same origin as the asymmetry shown in Fig. 4.2 does (see also Ref. [9]). We speculate that even if the superconductivity in the compounds consists of the preformed pairs or is in the crossover region between the BCS superconductivity and the Bose-Einstein condensation, the Bogoliubov wave functions would still be defined. If so, the electronic state of the vortex core in the compounds is understood as the Andreev scattering[48] and it is the coherent state. From our results based on the Bogoliubov wave functions, we conclude that the particle-hole asymmetry inside the vortex core observed in the experiments[18, 19] implies the corresponding existence of the vortex charging. According to another STM experiment by Renner *et al.*[25], the coherent electronic structure inside the core, observed as sharp structure of the LDOS, is smeared gradually by impurity doping. We predict that the vortex core charge decreases by impurity doping, because the charging is related to the sharp LDOS structure inside the vortex core in our scenario.

4.5 Summary

We investigated the electron density around a single vortex on the basis of the BdG theory. Its temperature dependence was presented. We expect that experimental data regarded as the vortex core charge will exhibit the temperature dependence as shown in Fig. 4.3. If such dependence is observed, those experimental data will become solid evidence of the vortex core charging. We discussed the microscopic charging mechanism, *which is independent of the slope in the density of states at the Fermi level*, by considering the CdGM states around the vortex. We pointed out the relation between the vortex bound states, probed potentially by STM, and the vortex core charging, based on the inherent particle-

hole asymmetry inside the vortex core *originated from the CdGM states of the vortex.*

Chapter 5

Conclusion

A fresh understanding of the electronic structure around vortices has been acquired since the success of the STM experiment by Hess *et al.* in 1989. It was steadily established that the electronic structure inside the vortex core in clean superconductors was quite different from the traditional normal-core electronic structure. From the theoretical point of view, a careful study based on scrupulous consideration of the Bogoliubov wave functions or Green's functions around a vortex is the only way to a steady understanding of the vortex structure in clean superconductors. On the basis of the non-perturbation approach, it was able to be revealed that anisotropy in the superconducting energy gap has significant consequences in the real space STM images and spectra around vortices. This opens a possibility that one could determine even the symmetry of the pairing function through the (energy dependent) imaging spectroscopy of a vortex by STM. The study presented in this thesis gave an actual example in which the theory was able to be comparable with the experiment on the existing material. It is expected that, future STM experiments are performed on various superconductors in the vortex state, so that potential ability of the STM blooms with future further development of theories.

Focusing on quantum-limit behavior, we were able to reveal essential properties of vortices which were concealed within the conventional non-quantum-limit analysis. Especially, it was found that the local density of states inside a vortex core generally has particle-hole asymmetry induced by the existence of the vortex itself. It would have implications for various physical phenomena related to vortices. As an example, the electric charging of a vortex core was discussed on the basis of the particle-hole asymmetry inside the core. The atomic-length-order oscillation of the Bogoliubov wave functions around the vortex and the particle-hole asymmetry inside the vortex core cooperatively give rise to the vortex core charge. It is not until we carefully consider the exact Bogoliubov wave functions around a vortex that the relation between the vortex core charge and the electronic structure around the vortex (or the vortex bound states) becomes clear. Future STM experiments are hopefully expected to investigate a vortex core focusing on particle-hole asymmetry inside the vortex core. A direct observation of the electric charge around a vortex by a new probe, the single-electron transistor scanning electrometer (SETSE)[122], also deserves a great deal of attention as a future hopeful experiment.

Vortices broadly appear in various situations around nature. They are of key

importance not only to the condensed matter physics, but also to the superfluid neutron star matter systems[98], the cosmology of the early Universe[123] and so forth. The vortices will keep giving us the variety of nature as physical subjects for both experimental and theoretical researches.

Acknowledgments

I am greatly grateful to Professor Kazushige Machida for stimulating my interest in the physics of superconductivity, his encouraging suggestion as colleague's idea and also as supervisor's advice, fruitful collaboration, and useful daily discussions. I owe the opportunity of nice start on my physics research to him.

I wish to express my special sincerity to Dr. Harald F. Hess. My work at the beginning of the doctoral course was motivated by his suggestion about the vortex structure related to his STM experiments. I would like to greatly thank him for fruitful suggestion, useful communication, sending experimental data of his original work, helpful discussions, and considerate correspondence, by which I have been encouraged certainly. I owe the start on my physics research to him also.

I would like to thank Dr. Masanori Ichioka, Mr. Naoki Enomoto, and Mr. Tomoya Isoshima for their collaboration. I am also grateful to Dr. Ichioka for critical discussions, and to Mr. Isoshima for his collaborative contribution to the results and the corresponding figures in the chapter 3.

I owe part of the present calculations (the quasiclassical calculation) to useful theoretical information from Dr. Nils Schopohl. I am exceedingly grateful to him for letting us have the opportunity to fruitfully utilize the Riccati equation developed by him.

I would like to thank Dr. Christophe Renner, Dr. Yukio Tanaka, Dr. Yoshifumi Morita, Dr. Masashige Matsumoto, Dr. Marcel Franz, Dr. Munehiro Nishida, Dr. Masahiko Machida, Dr. Akihiro Tanaka, Dr. Takafumi Kita, Dr. Yuji Matsuda, Dr. Mahito Kohmoto, Dr. Grigori E. Volovik, Dr. Ping Ao, Dr. Fabio V. De Blasio, Dr. Rudolf P. Hübener, Dr. Shoji Yamamoto, Dr. Andrei G. Lebed, Dr. Jiro Ozaki, Mr. Eiji Kaneshita, Mr. Mitsuaki Takigawa, Dr. Keita Kishigi, and Dr. Yoshiki Hori for useful discussions and/or correspondence in various respects.

Bibliography

- [1] A. L. Fetter and P. C. Hohenberg, in *Superconductivity*, edited by R. D. Parks (Marcel Dekker, New York, 1969), Chap. 14.
- [2] Y. Morita, K. Kohmoto, and K. Maki, *Int. J. Mod. Phys. B* **12**, 989 (1998).
- [3] C. Caroli, P. G. de Gennes, and J. Matricon, *Phys. Lett.* **9**, 307 (1964).
- [4] P. G. de Gennes, *Superconductivity of Metals and Alloys*, (Benjamin, New York, 1966), Chap. 5, p. 137.
- [5] See for a comprehensive review article, A. Khurana, *Phys. Today* **43**, No. 6, 17 (1990).
- [6] H. F. Hess, R. B. Robinson, R. C. Dynes, J. M. Valles, Jr., and J. V. Waszczak, *Phys. Rev. Lett.* **62**, 214 (1989).
- [7] M. Tinkham, *Introduction to Superconductivity*, 2nd ed. (McGraw-Hill, New York, 1996), p. 75.
- [8] H. F. Hess, in *Scanning Tunneling Microscopy*, edited by J. A. Stroscio and W. J. Kaiser (Academic Press, San Diego, 1993), Chap. 9, p. 427.
- [9] N. Hayashi, T. Isoshima, M. Ichioka and K. Machida, *Phys. Rev. Lett.* **80**, 2921 (1998).
- [10] N. Hayashi, M. Ichioka, and K. Machida, *J. Phys. Soc. Jpn.* **67**, 3368 (1998).
- [11] J. D. Shore, M. Huang, A. T. Dorsey, and J. P. Sethna, *Phys. Rev. Lett.* **62**, 3089 (1989).
- [12] H. F. Hess, R. B. Robinson, and J. V. Waszczak, *Phys. Rev. Lett.* **64**, 2711 (1990).
- [13] H. F. Hess, *Physica C* **185-189**, 259 (1991).
- [14] H. F. Hess, *Jpn. J. Appl. Phys. Series 9*, 270 (1993).
- [15] H. F. Hess, R. B. Robinson, and J. V. Waszczak, *Physica B* **169**, 422 (1991).
- [16] F. Gygi and M. Schlüter, *Phys. Rev. B* **43**, 7609 (1991).
- [17] F. Gygi and M. Schlüter, *Phys. Rev. Lett.* **65**, 1820 (1990); see also Sec. IV of Ref. [16].

- [18] I. Maggio-Aprile, Ch. Renner, A. Erb, E. Walker, and Ø. Fischer, *Phys. Rev. Lett.* **75**, 2754 (1995).
- [19] Ch. Renner, B. Revaz, K. Kadowaki, I. Maggio-Aprile, and Ø. Fischer, *Phys. Rev. Lett.* **80**, 3606 (1998).
- [20] R. Leadon and H. Suhl, *Phys. Rev.* **165**, 596 (1968).
- [21] J. Bardeen, R. Kümmel, A. E. Jacobs, and L. Tewordt, *Phys. Rev.* **187**, 556 (1969); W. Bergk and L. Tewordt, *Z. Phys.* **230**, 178 (1970).
- [22] L. Kramer and W. Pesch, *Z. Phys.* **269**, 59 (1974); see also W. Pesch and L. Kramer, *J. Low Temp. Phys.* **15**, 367 (1974).
- [23] R. J. Watts-Tobin, L. Kramer, and W. Pesch, *J. Low Temp. Phys.* **17**, 71 (1974).
- [24] For further articles of early theoretical work on the electronic structure of vortices, see references cited in a textbook (Ref. [8]).
- [25] Ch. Renner, A. D. Kent, Ph. Niedermann, Ø. Fischer, and F. Lévy, *Phys. Rev. Lett.* **67**, 1650 (1991).
- [26] For further other developments of the STM observation of vortices, see for example, S. Kashiwaya, M. Koyanagi, and A. Shoji, *Appl. Phys. Lett.* **61**, 1847 (1992); A. A. Golubov and U. Hartmann, *Phys. Rev. Lett.* **72**, 3602 (1994); A. P. Volodin, A. A. Golubov, and J. Aarts, *Z. Phys. B* **102**, 317 (1997).
- [27] A. W. Overhauser and L. L. Daemen, *Phys. Rev. Lett.* **62**, 1691 (1989).
- [28] L. L. Daemen and A. W. Overhauser, *Phys. Rev. B* **40**, 10778 (1989).
- [29] F. Gygi and M. Schlüter, *Phys. Rev. B* **41**, 822 (1990).
- [30] U. Klein, *Phys. Rev. B* **40**, 6601 (1989).
- [31] U. Klein, *Phys. Rev. B* **41**, 4819 (1990).
- [32] S. Ullah, A. T. Dorsey, and L. J. Buchholtz, *Phys. Rev. B* **42**, 9950 (1990).
- [33] B. Pöttinger and U. Klein, *Phys. Rev. Lett.* **70**, 2806 (1993).
- [34] N. Schopohl and K. Maki, *Phys. Rev. B* **52**, 490 (1995).
- [35] K. Maki, N. Schopohl, and H. Won, *Physica B* **204**, 214 (1995).
- [36] G. Eilenberger, *Z. Phys.* **214**, 195 (1968).
- [37] A. I. Larkin and Yu. N. Ovchinnikov, *Zh. Éksp. Teor. Fiz.* **55**, 2262 (1968) [*Sov. Phys. JETP* **28**, 1200 (1969)].
- [38] See for a review article of the quasiclassical theory, J. W. Serene and D. Rainer, *Phys. Rep.* **101**, 221 (1983).
- [39] M. Ichioka, N. Hayashi, N. Enomoto, and K. Machida, *Phys. Rev. B* **53**, 15316 (1996).

- [40] I am greatly indebted to H. F. Hess for bringing this similarity to our attention.
- [41] N. Hayashi, M. Ichioka, and K. Machida, Phys. Rev. Lett. **77**, 4074 (1996).
- [42] M. Ichioka, N. Hayashi, and K. Machida, Phys. Rev. B. **55**, 6565 (1997).
- [43] See for the Fermi surface of NbSe₂, R. Corcoran, P. Meeson, Y. Onuki, P. A. Probst, M. Springford, K. Takita, H. Harima, G. Y. Guo, and B. L. Gyorffy, J. Phys. Condens. Matter **6**, 4479 (1994).
- [44] In three dimensional systems with a general pairing, it is needed to take account of a phase-sensitively tunneling process when we consider STM results. See Y. Tanaka and S. Kashiwaya, Phys. Rev. Lett. **74**, 3451 (1995); M. Yamashiro, Y. Tanaka, Y. Tanuma, and S. Kashiwaya, J. Phys. Soc. Jpn. **67**, 3224 (1998).
- [45] M. Matsumoto and H. Shiba, J. Phys. Soc. Jpn. **64**, 3384 (1995); **64**, 4867 (1995); **65**, 2194 (1996). The electronic structure around a columnar defect was also investigated in M. Matsumoto, S. Kaneko, and N. Nishida, J. Phys. Soc. Jpn. **66**, 3211 (1997).
- [46] L. J. Buchholtz, M. Palumbo, D. Rainer, and J. A. Sauls, J. Low Temp. Phys. **101**, 1079 (1995); **101**, 1099 (1995).
- [47] M. Ichioka, N. Hayashi, N. Enomoto, and K. Machida, J. Phys. Soc. Jpn. **64**, 4547 (1995); M. Ichioka, N. Enomoto, N. Hayashi, and K. Machida, Phys. Rev. B **53**, 2233 (1996); K. Machida, M. Ichioka, N. Hayashi, and N. Enomoto, Physica C **263**, 428 (1996).
- [48] D. Rainer, J. A. Sauls, and D. Waxman, Phys. Rev. B **54**, 10094 (1996). I believe that a correct understanding on the electronic structure of vortices is presented in Introduction of their paper.
- [49] U. Klein, J. Low Temp. Phys. **69**, 1 (1987).
- [50] E. V. Thuneberg, J. Kurkijärvi, and D. Rainer, Phys. Rev. B **29**, 3913 (1984).
- [51] R. C. Dynes, V. Narayanamurti, and J. P. Garno, Phys. Rev. Lett. **41**, 1509 (1978).
- [52] N. Schopohl (unpublished); cond-mat/9804064.
- [53] For example, W. H. Press, S. A. Teukolsky, W. T. Vetterling, and B. P. Flannery, *Numerical Recipes in FORTRAN*, 2nd ed. (Cambridge University Press, London, 1992), p. 708.
- [54] D. Markowitz and L. P. Kadanoff, Phys. Rev. **131**, 563 (1963).
- [55] J. R. Clem, Phys. Rev. **148**, 392 (1966).
- [56] J. R. Clem, Ann. Phys. (N.Y.) **40**, 268 (1966).
- [57] K. Ishida, Y. Niino, G.-Q. Zheng, Y. Kitaoka, K. Asayama, and T. Ohtani, J. Phys. Soc. Jpn. **65**, 2341 (1996).

- [58] L. C. Hebel, Phys. Rev. **116**, 79 (1959).
- [59] H. F. Hess (private communication).
- [60] Strictly speaking, the states for θ in the vicinity of nodes are in the scattering (or extended) state, and $N(E, \mathbf{r}, \theta)$ is spread on the real space for these θ .
- [61] Y. D. Zhu, F. C. Zhang, and M. Sigrist, Phys. Rev. B **51**, 1105 (1995).
- [62] H. F. Hess, C. A. Murray, and J. V. Waszczak, Phys. Rev. B **50**, 16528 (1994).
- [63] H. F. Hess, C. A. Murray, and J. V. Waszczak, Phys. Rev. Lett. **69**, 2138 (1992).
- [64] C. A. Bolle, F. De La Cruz, P. L. Gammel, J. V. Waszczak, and D. J. Bishop, Phys. Rev. Lett. **71**, 4039 (1993).
- [65] H. Won and K. Maki, Europhys. Lett. **30**, 421 (1995); Phys. Rev. B **53**, 5927 (1996).
- [66] N. Enomoto, M. Ichioka, and K. Machida, J. Phys. Soc. Jpn. **66**, 204 (1997); M. Ichioka, N. Enomoto, and K. Machida, J. Phys. Soc. Jpn. **66**, 3928 (1997).
- [67] J. Shiraishi, M. Kohmoto, and K. Maki, cond-mat/9709310; cond-mat/9802067.
- [68] B. Keimer, W. Y. Shih, R. W. Erwin, J. W. Lynn, F. Dogan, and I. A. Aksay, Phys. Rev. Lett. **73**, 3459 (1994).
- [69] Ch. Renner, I. Maggio-Aprile, A. Erb, E. Walker, and Ø. Fischer, Proc. SPIE **2696B**, 322 (1996); I. Maggio-Aprile, Ch. Renner, A. Erb, E. Walker, and Ø. Fischer, J. Low Temp. Phys. **105**, 1129 (1996).
- [70] For example, C. C. Tsuei, J. R. Kirtley, C. C. Chi, L. S. Yu-Jahnes, A. Gupta, T. Shaw, J. Z. Sun, and M. B. Ketchen, Phys. Rev. Lett. **73**, 593 (1994).
- [71] See for a comprehensive review article, B. G. Levi, Phys. Today **48**, No. 11, 19 (1995).
- [72] Y. Morita, M. Kohmoto, and K. Maki, Phys. Rev. Lett. **78**, 4841 (1997); **79**, 4514(reply) (1997); see also M. Franz and M. Ichioka, Phys. Rev. Lett. **79**, 4513(comment) (1997).
- [73] P. I. Soininen, C. Kallin, and A. J. Berlinsky, Phys. Rev. B **50**, 13883 (1994).
- [74] Y. Wang and A. H. MacDonald, Phys. Rev. B **52**, 3876 (1995).
- [75] In lattice models, it is natural to consider an (extended) s -wave pairing in addition to the d -wave one even when on-site (s -wave pairing) interaction is repulsive. For articles on the induced s -wave component of the pair potential around a vortex in d -wave superconductors, see D. L. Feder and C. Kallin, Phys. Rev. B **55**, 559 (1997), and references cited therein.

- [76] A calculation for the electronic structure around vortices in a d -wave superconductor was recently performed on t - J model, where a possible relation between the vortex bound states and an induced s -wave component of the pair potential was pointed out. A. Himeda, M. Ogata, Y. Tanaka, and S. Kashiwaya, *J. Phys. Soc. Jpn.* **66**, 3367 (1997).
- [77] Y. De Wilde, M. Iavarone, U. Welp, V. Metlushko, A. E. Koshelev, I. Aranson, G. W. Crabtree, and P. C. Canfield, *Phys. Rev. Lett.* **78**, 4273 (1997).
- [78] Y. Maeno, H. Hashimoto, K. Yoshida, S. Nishizaki, T. Fujita, J. G. Bednorz, and F. Lichtenberg, *Nature* **372**, 532 (1994).
- [79] T. Oguchi, *Phys. Rev. B* **51**, 1385 (1995).
- [80] D. J. Singh, *Phys. Rev. B* **52**, 1358 (1995).
- [81] M. Sigrist and M. E. Zhitomirsky, *J. Phys. Soc. Jpn.* **65**, 3452 (1996).
- [82] K. Machida, M. Ozaki, and T. Ohmi, *J. Phys. Soc. Jpn.* **65**, 3720 (1996).
- [83] C. Caroli and J. Matricon, *Phys. Kondens. Mater.* **3**, 380 (1965).
- [84] S. J. Hagen, A. W. Smith, M. Rajeswari, J. L. Peng, Z. Y. Li, R. L. Greene, S. N. Mao, X. X. Xi, S. Bhattacharya, Q. Li, and C. J. Lobb, *Phys. Rev. B* **47**, 1064 (1993); G. D'Anna, V. Berseth, L. Forró, A. Erb, and E. Walker, cond-mat/9811106; V. N. Narozhnyi, J. Freudenberger, V. N. Kochetkov, K. A. Nenkov, G. Fuchs, and K.-H. Müller, cond-mat/9811273. Useful review and discussion of both experiments and theories are given in these papers. The above recent paper by D'Anna *et al.* pointed out that even if one considers the Hall *conductivity* σ_{xy} , the pinning effect cannot be excluded from the consideration and rather the pinning must play an important role in the Hall effect.
- [85] T. Nagaoka, Y. Matsuda, H. Obara, A. Sawa, T. Terashima, I. Chong, M. Takano, and M. Suzuki, *Phys. Rev. Lett.* **80**, 3594 (1998); see also Y. Matsuda, T. Nagaoka, G. Suzuki, K. Kumagai, M. Suzuki, M. Machida, M. Sera, M. Hiroi, and N. Kobayashi, *Phys. Rev. B* **52**, 15749 (1995).
- [86] K. Krishana, J. M. Harris, and N. P. Ong, *Phys. Rev. Lett.* **75**, 3529 (1995). See also, K. Krishana *et al.*, *Science* **277**, 83 (1997).
- [87] See, e.g., R. Corcoran, N. Harrison, S. M. Hayden, P. Meeson, M. Springford, and P. J. van der Wel, *Phys. Rev. Lett.* **72**, 701 (1994).
- [88] See, e.g., A. van Otterlo *et al.*, *Phys. Rev. Lett.* **75**, 3736 (1995); N. B. Kopnin and G. E. Volovik, *Phys. Rev. B* **57**, 8526 (1998); A. I. Larkin and Yu. N. Ovchinnikov, *Phys. Rev. B* **57**, 5457 (1998); M. Hayashi, *J. Phys. Soc. Jpn.* **67**, 3372 (1998). These authors try to understand vortex dynamics in terms of the quasiparticle excitations in a vortex core.
- [89] G. E. Volovik, *JETP Lett.* **58**, 455 (1993).
- [90] For the KP effect in the d -wave pair case, see Ref. [39]

- [91] S. G. Doettinger, R. P. Huebener, and S. Kittelberger, Phys. Rev. B **55**, 6044 (1997).
- [92] J. E. Sonier, R. F. Kiefl, J. H. Brewer, J. Chakhalian, S. R. Dunsiger, W. A. MacFarlane, R. I. Miller, A. Wong, G. M. Luke, and J. W. Brill, Phys. Rev. Lett. **79**, 1742 (1997).
- [93] J. E. Sonier, J. H. Brewer, R. F. Kiefl, D. A. Bonn, S. R. Dunsiger, W. N. Hardy, Ruixing Liang, W. A. MacFarlane, R. I. Miller, T. M. Riseman, D. R. Noakes, C. E. Stronach, and M. F. White Jr., Phys. Rev. Lett. **79**, 2875 (1997).
- [94] M. Franz and Z. Tešanović, Phys. Rev. Lett. **80**, 4763 (1998).
- [95] N. Hayashi, M. Ichioka, and K. Machida, Phys. Rev. B **56**, 9052 (1997).
- [96] S. Giorgini, J. Boronat, and J. Casulleras, Phys. Rev. Lett. **77**, 2754 (1996), and earlier references therein.
- [97] E. H. Brandt, Phys. Rev. Lett. **78**, 2208 (1997).
- [98] F. V. De Blasio and Ø. Elgarøy, nucl-th/9808057. The first investigation of a vortex line in superfluid neutron star matter systems based on the BdG theory was done by De Blasio and Elgarøy. It is probable for the quantum limit to be realized in those systems.
- [99] M. Yethiraj, D. McK. Paul, C. V. Tomy, and E. M. Forgan, Phys. Rev. Lett. **78**, 4849 (1997).
- [100] M. R. Eskildsen, P. L. Gammel, B. P. Barber, A. P. Ramirez, D. J. Bishop, N. H. Andersen, K. Mortensen, C. A. Bolle, C. M. Lieber, and P. C. Canfield, Phys. Rev. Lett. **79**, 487 (1997).
- [101] J. E. Sonier, R. F. Kiefl, J. H. Brewer, D. Bonn, S. Dunsiger, R. Liang, R. I. Miller, D. R. Noakes, and C. E. Stronach, cond-mat/9806064.
- [102] A. Yaouanc, P. Dalmas de Réotier, and E. H. Brandt, Phys. Rev. B **55**, 11107 (1997).
- [103] D. I. Khomskii and A. Freimuth, Phys. Rev. Lett. **75**, 1384 (1995).
- [104] G. Blatter, M. V. Feigel'man, V. B. Geshkenbein, A. I. Larkin, and A. van Otterlo, Phys. Rev. Lett. **77**, 566 (1996).
- [105] From the historical point of view, the vortex core charge was discussed in the context of the sign change problem of the Hall conductivity in the mixed state. The proposed Hall force originated from the core charge is *not* an electromagnetic force, but a hydrodynamic or a topological one (see refs. [103] and [117]). It is, however, controversial that the transverse force proposed in ref. [117] is of topological origin. See P. Ao and X.-M. Zhu, Physica C **282-287**, 367 (1997); and Refs. [119] and [121].
- [106] K.-U. Neumann, F. V. Kusmartsev, H.-J. Lauter, O. Schärpf, T. J. Smith, and K. R. A. Ziebeck, Eur. Phys. J. B **1**, 5 (1998).

- [107] F. V. Kusmartsev, K.-U. Neumann, O. Schärpf, and K. R. A. Ziebeck, *Europhys. Lett.* **42**, 547 (1998).
- [108] D. I. Khomskii and F. V. Kusmartsev, *Phys. Rev. B* **46**, 14245 (1992).
- [109] Y. Tanaka, A. Hasegawa, and H. Takayanagi, *Solid State Commun.* **85**, 321 (1993); *Physica B* **194-196**, 1761 (1994); Y. Tanaka, S. Kashiwaya, and H. Takayanagi, *Jpn. J. Appl. Phys.* **34**, 4566 (1995). In these papers, a multiple winding number vortex (trapped by a quantum dot) was discussed.
- [110] T. Isoshima and K. Machida, *J. Phys. Soc. Jpn.* **66**, 3502 (1997); **67**, 1840 (1998). The trapped dilute Bose gas systems were discussed there.
- [111] Y. Morita, M. Kohmoto, and K. Maki, *Europhys. Lett.* **40**, 207 (1997).
- [112] M. Kato and K. Maki, cond-mat/9810187.
- [113] See, e.g., A. W. Overhauser, *Phys. Rev.* **167**, 691 (1968).
- [114] Equation (4.6) cannot be appropriate for the solutions of vortices, when we consider the vortex lattice structure in the 2D-Hubbard model *with just half filling* where we cannot determine whether the dominant carriers are the electrons or holes. Indeed, in this case, the LDOS exhibits perfect particle-hole symmetry inside the vortex core and the core charge is zero. M. Ichioka, (private communication).
- [115] A. van Otterlo, M. V. Feigel'man, V. B. Geshkenbein, and G. Blatter, *Phys. Rev. Lett.* **75**, 3736 (1995).
- [116] See, e.g., comments and replies, P. Ao, *Phys. Rev. Lett.* **80**, 5025 (1998); N. B. Kopnin and G. E. Volovik, *Phys. Rev. Lett.* **80**, 5026 (1998); H. E. Hall and J. R. Hook, *Phys. Rev. Lett.* **80**, 4356 (1998); C. Wexler *et al.*, *Phys. Rev. Lett.* **80**, 4357 (1998); E. B. Sonin, *Phys. Rev. Lett.* **81**, 4276 (1998); C. Wexler *et al.*, *Phys. Rev. Lett.* **81**, 4277 (1998).
- [117] M. V. Feigel'man, V. B. Geshkenbein, A. I. Larkin, and V. M. Vinokur, *JETP Lett.* **62**, 834 (1995).
- [118] N. B. Kopnin, G. E. Volovik, and Ü. Parts, *Europhys. Lett.* **32**, 651 (1995).
- [119] G. E. Volovik, *JETP Lett.* **65**, 676 (1997).
- [120] N. B. Kopnin, *Phys. Rev. B* **54**, 9475 (1996).
- [121] A discussion of the vortex dynamics based on the exact wave functions has been given in, J. Dziarmaga, *Phys. Rev. B* **53**, 6572 (1996); F. Gaitan, *Phys. Rev. B* **51**, 9061 (1995); see also F. Gaitan, *Phys. Rev. A* **58**, 1665 (1998); F. Gaitan, quant-ph/9809008. However, a relation between the spectral flow theory and the temperature dependence of the carrier density at the vortex center is not yet clear.
- [122] M. J. Yoo, T. A. Fulton, H. F. Hess, R. L. Willett, L. N. Dunkleberger, R. J. Chichester, L. N. Pfeiffer, and K. W. West, *Science* **276**, 579 (1997).
- [123] T. D. C. Bevan, A. J. Manninen, J. B. Cook, J. R. Hook, H. E. Hall, T. Vachaspati, and G. E. Volovik, *Nature* **386**, 689 (1997); see also P. Ao, hep-ph/9801241(comment).